






## Evolution of the ZTF SLRN-2020 star-planet merger

RICARDO YARZA <sup>1,\*</sup> MORGAN MACLEOD <sup>2,3</sup> BENJAMIN IDINI <sup>1</sup> RUTH MURRAY-CLAY <sup>1</sup> AND  
ENRICO RAMIREZ-RUIZ <sup>1</sup>

<sup>1</sup>*Department of Astronomy and Astrophysics, University of California, Santa Cruz, CA 95064, USA*

<sup>2</sup>*Center for Astrophysics, Harvard & Smithsonian, 60 Garden Street, MS-16, Cambridge, MA 02138, USA*

<sup>3</sup>*Institute for Theory and Computation, Harvard & Smithsonian, 60 Garden Street, MS-51, Cambridge, MA 02138, USA*

### ABSTRACT

We model the optical and infrared transient ZTF SLRN-2020, previously associated with a star-planet merger. We consider the scenario in which orbital decay via tidal dissipation led to the merger, and find that tidal heating within the star was likely unobservable in the archival image of the system taken 12 yr before the merger. The observed dust formation months before the merger is consistent with a planet of mass  $M_p \gtrsim 5 M_J$  ejecting material as it skims the stellar surface. This interaction gradually intensifies, leading to significant mass ejection on a dynamical timescale ( $\approx$  hours) as the planet plunges into the stellar interior. Part of the recombination transient associated with this dynamical mass ejection might be inaccessible to the optical observations because its duration ( $\approx$  hours) is comparable to the cadence. Correspondingly, the observed duration of the transient  $\approx 100$  d is inconsistent with a single episode of dynamical mass ejection. Instead, the transient could be powered by the recombination of  $3.4 \times 10^{-5} M_\odot$  of hydrogen in an outflow, or the contraction of an inflated envelope of mass  $\approx 10^{-6} M_\odot$  that formed during the merger. The observed ejecta mass 320 d after the peak of the optical transient is  $\approx 1.3 \times 10^{-4} M_\odot$ , consistent with the idea that a fraction of the ejecta might be unobservable in the light curve. Energetically, this post-merger ejecta mass suggests a planet at least as massive as Jupiter. Our results suggest that ZTF SLRN-2020 was the result of a merger between a star close to the main sequence and a planet with mass at least several times that of Jupiter.

### 1. INTRODUCTION

The observed orbital configurations of planetary systems imply that a large fraction of the known exoplanets will merge with their host stars at some point during their evolution (F. A. Rasio et al. 1996; E. Villaver & M. Livio 2007, 2009; B. Jackson et al. 2009; B. Levrard et al. 2009; S. Matsumura et al. 2010; J. Nordhaus et al. 2010; J. K. Carlberg et al. 2011; M. Kunitomo et al. 2011; B. D. Metzger et al. 2012; A. J. Mustill & E. Villaver 2012; J. Nordhaus & D. S. Spiegel 2013; K. C. Schlaufman & J. N. Winn 2013; E. Villaver et al. 2014; T. Matsakos & A. Königl 2015; C. Damiani & R. F. Díaz 2016; D. Veras 2016; I. Rapoport et al. 2021; S. R. Kane 2023; A. Mustill 2024). The main mechanisms leading to these mergers are tidal dissipation of orbital energy, stellar expansion during the post-main-sequence, and dynamical interactions. Roughly 0.5% of sunlike stars host a hot Jupiter (A. W. Howard et al. 2012). The occurrence rate of hot Jupiters appears to decrease with stellar age along the main sequence, suggesting that tidal dissipation is efficient enough to lead to mergers on timescales comparable to the main sequence lifetime (J. H. Hamer & K. C. Schlaufman 2019; S. Miyazaki & K. Masuda

2023). On average, each sunlike star has  $\approx 1$  planet with radius between  $1 R_\oplus$  and  $20 R_\oplus$  and period  $< 400$  d (W. Zhu & S. Dong 2021); at such orbital periods, tides and post-main-sequence expansion often lead to mergers. Estimates for the merger rate in the Galaxy range from one every few years to a few per year (B. D. Metzger et al. 2012; M. MacLeod et al. 2018a; A. V. Popkov & S. B. Popov 2019; K. De et al. 2023).

A star-planet merger potentially produces a range of observable effects. The angular momentum of the orbit of the planet is transferred to the star, increasing its spin rate (L. Siess & M. Livio 1999a,b; M. Livio & N. Soker 2002; A. Massarotti et al. 2008; J. K. Carlberg et al. 2009, 2011, 2012, 2013; M. Zhang & K. Penev 2014; G. Privitera et al. 2016a; A. Qureshi et al. 2018; A. Oetjens et al. 2020; A. P. Stephan et al. 2020; R. M. Cabezón et al. 2023; S.-S. Guo 2023; M. Y. M. Lau et al. 2025). The deposition of planetary material in the star temporarily changes the stellar atmospheric abundances (J. B. Alexander 1967; G. Laughlin & F. C. Adams 1997; E. Sandquist et al. 1998; L. Siess & M. Livio 1999a,b; R. G. Gratton et al. 2001; J. Montalbán & R. Rebolo 2002; E. L. Sandquist et al. 2002; A. M. Cody & D. D. Sasselov 2005; J. K. Carlberg et al. 2012, 2013; C. Aguilera-Gómez et al. 2016a,b; T. Nagar et al. 2020; M. Soares-Furtado et al. 2021; J. Sevilla et al. 2022; R. M.

\* NASA FINESST Fellow

Cabezón et al. 2023; D. Xie et al. 2023; M. Y. M. Lau et al. 2025; C. E. O’Connor & D. Lai 2025; B. M. T. B. Soares et al. 2025), which could explain unusual abundance patterns in a few systems (G. Israelian et al. 2001; S. L. Li et al. 2008; J. K. Carlberg et al. 2010; M. Adamów et al. 2012; L. Spina et al. 2015; E. Tognelli et al. 2016; C. Saffe et al. 2017; S. Oh et al. 2018; R. P. Church et al. 2020; J. Yana Galarza et al. 2021; P. Miquelarena et al. 2024; J. Yana Galarza et al. 2024). Broadly,  $\approx 5\%$  of main-sequence stars have abundance patterns consistent with a previous merger with a planet (A. Behrard et al. 2023; F. Liu et al. 2024). A star-planet merger could also change the magnetic field of the star (L. Siess & M. Livio 1999b; G. Privitera et al. 2016c). Overall, the timescales over which these rotational, magnetic, and chemical signatures remain observable depend on mixing and angular momentum transport within the star, two processes that remain poorly understood (G. Privitera et al. 2016a; J. Sevilla et al. 2022).

Until recently, the observational evidence for star-planet mergers had been exclusively indirect: present-day orbital configurations imply future mergers, while stars with observed anomalous properties suggest past mergers, with no directly observed connection from pre- to post-merger systems. The indirect evidence for star-planet mergers suffers from the fact that many non-merger processes can produce signatures similar to mergers. For example, stellar chemical anomalies can result from stellar internal processes (A. G. W. Cameron & W. A. Fowler 1971; J. K. Carlberg et al. 2013; H.-L. Yan et al. 2018; A. R. Casey et al. 2019; C. Aguilera-Gómez et al. 2020; M. Sayeed et al. 2024) or the intrinsic variability in stellar compositions (A. Behrard et al. 2023; C. Saffe et al. 2024; N. H. Soliman & P. F. Hopkins 2025; Q. Sun et al. 2025). These challenges further motivate the search for the transients produced by star-planet mergers in real time.

Multiple studies have modeled the transients produced by star-planet mergers (e.g., E. Bear et al. 2011; B. D. Metzger et al. 2012; A. Kashi & N. Soker 2017; B. D. Metzger et al. 2017; R. Yamazaki et al. 2017; M. MacLeod et al. 2018a; A. Kashi et al. 2019; T. Matsumoto & B. D. Metzger 2022; C. E. O’Connor et al. 2023). The primary mechanism responsible for optical emission is the recombination of hydrogen in an outflow of increasing strength as the star and planet approach coalescence over the course of  $\approx$  weeks (B. D. Metzger et al. 2012). When the planet finally plunges into the stellar interior on a dynamical timescale  $\approx$  hours, a mass ejection event likely produces a bright recombination transient with a duration comparable to a few orbital periods (B. D. Metzger et al. 2012; R. Yamazaki et al. 2017). The star radiates energy deposited deeper in the interior over the course of the much longer Kelvin–Helmholtz time (B. D. Metzger et al. 2012, 2017; M. MacLeod et al. 2018a; C. E. O’Connor et al. 2023). Hydrodynamical simulations are consistent with this overall picture (E. L. Sandquist et al.

2002; J. E. Staff et al. 2016; M. Kramer et al. 2020; R. M. Cabezón et al. 2023; M. Y. M. Lau et al. 2025).

K. De et al. (2023) discovered the infrared and optical transient ZTF SLRN-2020 and interpreted it as a star-planet merger, providing the first real-time observation of such an event. R. M. Lau et al. (2025) observed the merger remnant roughly two years later. The star-planet merger interpretation of this transient relies in part on its qualitative similarity to luminous red novae (LRNe), a transient class associated with the mergers of two stars (R. Tylenda et al. 2011; N. Ivanova et al. 2013). However, the radiated energy and ejecta mass of ZTF SLRN-2020 are smaller by a factor of roughly a hundred, suggesting a merger between a star and a much smaller companion.

Here we model the evolution of ZTF SLRN-2020. Section 2 summarizes the observations of ZTF SLRN-2020 (K. De et al. 2023; R. M. Lau et al. 2025), including the progenitor system and the outburst. Section 3 discusses the evolution of the system before the merger, which we model as tidal decay of the planetary orbit. Section 4 discusses the evolution of the system once the star and planet come into contact. The planet shocks and ejects stellar material near the surface; this interaction gradually intensifies until the planet is fully immersed in the star. Section 5 compares ZTF SLRN-2020 to stellar mergers and discusses the potential radiative processes responsible for the transient. Section 6 combines the results of previous sections to place energetic constraints on the mass of the planet.

## 2. SUMMARY OF OBSERVATIONS

Observations of ZTF SLRN-2020 include (i) archival near-infrared images of the progenitor star at the  $-12$  yr epoch (defined with respect to the peak of the optical transient), (ii) mid-infrared photometry starting at the  $-244$  d epoch, with a cadence of a few months, (iii) optical photometry for  $-30$  d  $\lesssim t \lesssim 150$  d, with a cadence of a few days, and (iv) infrared spectroscopy of the merger remnant at the 830 d epoch.

ZTF SLRN-2020 is located in the galactic disk, a distance

$$d \approx 4 \text{ kpc} \quad (1)$$

from Earth. Figure 1 from K. De et al. (2023) shows the optical and infrared light curves. Their Figure 2 shows the bolometric properties (see also Figure 5). We describe the observations in more detail below.

### 2.1. Progenitor

The progenitor star appears in  $H$  and  $K$  images from the United Kingdom Infrared Telescope (UKIRT) survey of the galactic plane (A. Lawrence et al. 2007), taken at the  $-12$  yr epoch. Multiple surveys covered the location of the progenitor, including PanSTARRS1 (K. C. Chambers et al. 2016), Gaia (Gaia Collaboration et al. 2016, 2021), and POSS-II (I. N. Reid et al. 1991), but none of them detected it. The position of the progenitor in

the HR diagram, as determined by the UKIRT images, is consistent with evolutionary tracks in the mass range  $0.8 \lesssim M_*/M_\odot \lesssim 1.5$  (K. De et al. 2023), although there are significant photometric errors. The  $1 M_\odot$  track is consistent with the observed progenitor for stellar radii between  $1 R_\odot$  and  $4 R_\odot$ , suggesting a star on or close to the main sequence. R. M. Lau et al. (2025) observed the source at the 830 d epoch, and estimated an intrinsic stellar luminosity  $L_* \approx 0.3 L_\odot$ , corresponding to a  $\approx 0.7 M_\odot$  main-sequence star. However, it is possible that dust is obscuring a slightly more luminous (i.e., more massive) star. The planet is not observable in the archival image; K. De et al. (2023) inferred its presence from the properties of the transient, so there are no direct constraints on its properties.

We will use a sunlike star ( $1 M_\odot$ ,  $1 R_\odot$ ) in our analysis. We present our calculations including the dependence on stellar mass and radius, so that they can be scaled to different stars. Some of our analysis requires knowledge of the internal structure of the star, which we calculate using the `1M_pre_ms_to_wd` inlist from the modules for experiments in stellar astrophysics (MESA; B. Paxton et al. 2011, and additional citations in the software section).

### 2.2. Pre-merger dust and infrared brightening

The source began to form dust and gradually brighten in the infrared around  $\approx 200$  d before the peak of the optical transient (see the WISE data points in Figure 1 from K. De et al. 2023). K. De et al. (2023) fit the infrared spectral energy distribution (SED) to estimate the mass of the dust around the source. Assuming a dust-to-gas mass ratio  $10^{-2}$ , they estimated a total (dust plus gas) ejecta mass of

$$M_{\text{ej}}(t = -244 \text{ d}) \approx 2.8 \times 10^{-5} M_\odot \left( \frac{d}{4 \text{ kpc}} \right)^2, \quad (2)$$

$$M_{\text{ej}}(t = -44 \text{ d}) \approx 10^{-4} M_\odot \left( \frac{d}{4 \text{ kpc}} \right)^2 \quad (3)$$

at the  $t = -244$  d and  $t = -44$  d epochs, respectively, where  $t = 0$  corresponds to the peak of the optical transient.

### 2.3. Optical transient

The optical luminosity increased significantly over the course of approximately ten days, reaching a peak at  $1.3 \times 10^{35} \text{ erg s}^{-1}$  that lasted about 25 d. After that, the transient faded by about an order of magnitude over 150 d (Figure 5). The total radiated energy over this period was

$$E_{\text{rad}} \approx 6 \times 10^{41} \text{ erg} \left( \frac{d}{4 \text{ kpc}} \right)^2. \quad (4)$$

K. De et al. (2023) estimated the bolometric properties from the optical peak to  $\approx 120$  d post-peak by fitting a

blackbody function to the ZTF and ATLAS photometry; see Section 13 of their supplemental information for more details. They also estimated the properties of the dust that formed around the remnant as a result of the merger using SEDs at the 120 d and 320 d epochs (see their extended data table 3). They found that the dust was expanding at a speed  $\approx 35 \text{ km s}^{-1}$ .

R. M. Lau et al. (2025) reanalyzed the optical and infrared SED of ZTF SLRN-2020 SED at 320 d and arrived at new estimates for the properties of the dust surrounding the remnant. Their model of the dust assumes that it is distributed in a spherical shell. The parameters of this shell, such as the inner radius, temperature, and optical depth are free parameters (see their table 3 for their best-fit values). Assuming a dust-to-gas mass ratio  $10^{-2}$ , they estimated a total (dust plus gas) ejecta mass of

$$\log_{10} \left( \frac{M_{\text{ej}}(t = 320 \text{ d})}{M_\odot} \right) = -3.89_{-3.21}^{+0.29}. \quad (5)$$

### 2.4. Remnant at 830 d

R. M. Lau et al. (2025) observed ZTF SLRN-2020 at 830 d using JWST and Gemini North. From the SED, they estimated  $\approx 10^{-9} M_\odot$  of warm ( $\approx 700$  K) gas around the remnant. They suggested that this gas forms an accretion disk around the remnant, based on their detection of  $^{12}\text{CO}$  and  $\text{Br}\alpha$  emission. They also constrained the properties of the progenitor and reanalyzed the 320 d SED, as we discussed above.

## 3. PRE-MERGER EVOLUTION

We will discuss the evolution of the system before the star and the planet come into contact, and determine the observability of the star-planet interaction at the time of the archival images of the progenitor (12 yr before the transient).

The presence of dust in the months prior to the main outburst suggests that the merger was the culmination of an escalating interaction on a timescale of  $\gtrsim$  months. Therefore, we focus on tidal dissipation as the likely mechanism that led to the merger. Orbital decay has been observed for WASP-12 b (G. Maciejewski et al. 2016; K. C. Patra et al. 2017; G. Maciejewski et al. 2018; A. Bailey & J. Goodman 2019; S. W. Yee et al. 2020; J. D. Turner et al. 2021; P. Leonardi et al. 2024) and Kepler-1658 b (S. Vissapragada et al. 2022), although the exact mechanism of tidal dissipation which would explain the observed rates of decay remains unclear (N. N. Weinberg et al. 2024; A. J. Barker et al. 2024; S. C. Millholland et al. 2025). We will begin by modeling the pre-merger orbital evolution of the system subject to tidal dissipation.

### 3.1. Tidal orbital decay

The orbital period of the close-in (orbital separation  $\approx$  stellar radius) planet is

$$P_{\text{orb}} = 2\pi (GM_{\star}/a^3)^{-1/2} \approx 2.8 \text{ h } (M_{\star}/M_{\odot})^{-1/2} (a/R_{\odot})^{3/2}, \quad (6)$$

where  $G$  is the gravitational constant,  $M_{\star}$  is the mass of the star, and  $a$  is the orbital separation. The orbital energy is, assuming a circular orbit,

$$E_{\text{orb}} = -\frac{GM_{\star}M_{\text{p}}}{2a} = -1.8 \times 10^{45} \text{ erg } \left(\frac{M_{\star}}{M_{\odot}}\right) \left(\frac{M_{\text{p}}}{M_{\text{J}}}\right) \left(\frac{a}{R_{\odot}}\right)^{-1}, \quad (7)$$

where  $M_{\text{p}}$  is the mass of the planet and  $M_{\text{J}}$  is the mass of Jupiter. Tides dissipate orbital energy at a rate

$$\begin{aligned} \dot{E}_{\text{tide}} &= -\frac{9}{2Q'_{\star}} \left(\frac{M_{\text{p}}}{M_{\star}}\right) \left(\frac{R_{\star}}{a}\right)^5 n E_{\text{orb}} \\ &= 13 L_{\odot} \left(\frac{M_{\text{p}}}{M_{\text{J}}}\right)^2 \left(\frac{M_{\star}}{M_{\odot}}\right)^{1/2} \left(\frac{R_{\star}}{R_{\odot}}\right)^5 \left(\frac{Q'_{\star}}{10^5}\right)^{-1} \\ &\quad \times \left(\frac{a}{R_{\odot}}\right)^{-15/2}, \end{aligned} \quad (8)$$

where  $n \equiv 2\pi/P_{\text{orb}}$  is the orbital mean motion and  $Q'_{\star}$  is the modified tidal quality factor of the star, which parametrizes the strength of the mechanism responsible for the tidal dissipation. A large  $Q'_{\star}$  corresponds to weak dissipation, and a small  $Q'_{\star}$  to strong dissipation (for a review of tidal dissipation in stars and giant planets, see [G. I. Ogilvie 2014](#)). The quality factor likely varies by several orders of magnitude depending on the properties of the star, planet, and the orbit ([A. J. Barker 2020](#)). Here, we keep  $Q'_{\star}$  as a free parameter with a power-law dependence on orbital period,

$$Q'_{\star} \propto P_{\text{orb}}^{\alpha}. \quad (9)$$

The timescale of orbital decay is

$$\tau_{\text{tide}} = -\int_0^a \frac{da'}{\dot{a}'} = \frac{2}{13 + 3\alpha} \frac{E_{\text{orb}}}{\dot{E}_{\text{tide}}}. \quad (10)$$

We also will consider also consider a range of constant quality factors between  $10^4$  and  $10^8$ . [K. Penev et al. \(2018\)](#) observationally constrained the tidal quality factor using the observed rotation rates of a sample of hot-Jupiter host stars. [S. C. Millholland et al. \(2025\)](#) did a similar experiment using the steady-state distribution of planetary orbital parameters. Under the assumption that the planets had tidally increased the rotation rate

of their stars on a timescale equal to the age of the stars, [K. Penev et al. \(2018\)](#) found a tidal quality factor

$$Q'_{\star, \text{Penev}} = \max \left[ 3.52 \times 10^6 \left(\frac{P_{\text{orb}}}{1 \text{ d}}\right)^{-3.1}, 10^5 \right], \quad (11)$$

which is broadly consistent with the later findings of [S. C. Millholland et al. \(2025\)](#) (see their Figure 7). We also consider this empirical tidal quality factor in our analysis, noting that population-level patterns do not necessarily predict the behavior of individual systems because the tidal quality factor might vary by orders of magnitude across systems.

### 3.2. Observability of tidal heating

Here we determine whether tidal heating changes the appearance of the star before the merger. There are two requirements for tidal heating to be observable: one, that the tidal energy deposition rate be comparable to the intrinsic stellar luminosity; and two, that the star respond to the tidal energy dissipated in its interior on a timescale shorter than the orbital decay time. For quality factors  $Q'_{\star} \lesssim 10^6 (M_{\text{p}}/M_{\text{J}})^2$ , the tidal energy dissipation rate is greater than the stellar luminosity when  $a \approx R_{\star}$ .

These requirements relate not only to the magnitude of the heating, but also to its location within the star ([P. Podsiadlowski 1996](#)). To illustrate the latter, consider a process which dissipates energy close to the center of the star (e.g., internal gravity waves). In order to expand, the heated material must share its energy with the layers above. As a result, heating will change the (quasi)hydrostatic stellar structure on the timescale on which the heating changes the total energy of the star,

$$\tau_{\text{heat, global}} = \dot{E}_{\text{tide}}^{-1} \int_0^{M_{\star}} c_p T dM \approx \frac{GM_{\star}^2}{2R_{\star} \dot{E}_{\text{tide}}}, \quad (12)$$

where  $c_p$  is the specific heat capacity,  $T$  is the temperature, and we approximated the internal energy of the star as  $0.5GM_{\star}^2/R_{\star}$ . This timescale is always longer than the timescale of orbital decay,

$$\approx \frac{GM_{\star}M_{\text{p}}}{a\dot{E}_{\text{tide}}}, \quad (13)$$

because the energy in the orbit is smaller than the energy in the star by a factor  $\approx (M_{\text{p}}/M_{\star}) \ll 1$ . Therefore, central heating is unlikely to be observable before the merger.

In contrast, consider a process that heats the outermost  $M_{\text{heat}}$  of the star (e.g., turbulent dissipation of the equilibrium tide). The timescale over which this region will expand is the local heating time

$$\tau_{\text{heat}} \approx f \frac{GM_{\star}M_{\text{heat}}}{2R_{\star} \dot{E}_{\text{tide}}}, \quad (14)$$

where  $f \lesssim 1$  is a numerical factor accounting for the fact that  $c_p T < GM_{\star}/R_{\star}$  in the outer regions of the star. If

the energy is deposited close to the surface (i.e.,  $M_{\text{heat}} \ll M_*$ ), the local heating time can be much shorter than the global one. We can combine equations (10) and (14) to relate the thermal and orbital decay timescales,

$$\tau_{\text{tide}} \approx f^{-1} \frac{2}{13 + 3\alpha} \frac{M_p}{M_{\text{heat}}} \frac{R_*}{a} \tau_{\text{heat}}. \quad (15)$$

Equation (8) shows that  $\dot{E}_{\text{tide}}/L_* \propto M_p^2$ , and equation (15) shows that  $\tau_{\text{tide}}/\tau_{\text{heat}} \propto M_p$ , so heating from more massive planets is more likely to be observable.

Figure 1 shows tidal evolution tracks in the plane defined by  $\dot{E}_{\text{tide}}/L_*$  and  $\tau_{\text{tide,merge}}/\tau_{\text{heat}}$ , where

$$\tau_{\text{tide,merge}}(a) \equiv \tau_{\text{tide}}(a) - \tau_{\text{tide}}(R_* + R_p) \quad (16)$$

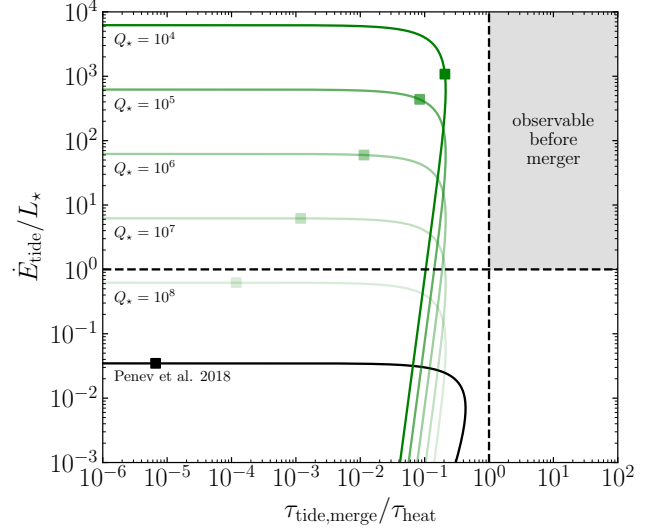
is the tidal orbital decay time to the orbital separation at which the star and the planet come into contact. We use a sunlike star with a  $10 M_J$  companion. We assume  $f = 0.2$  and  $M_{\text{heat}} = 2 \times 10^{-2} M_\odot$ , corresponding to a mechanism that deposits heat near the base of the outer convective zone. Initially,  $\tau_{\text{tide,merge}}/\tau_{\text{heat}} \propto a^{-1}$ , as in equation (15). However, as the orbital separation approaches  $R_*$ ,  $\tau_{\text{tide,merge}}$  approaches zero while  $\tau_{\text{heat}}$  approaches a constant positive value, so all curves bend toward the left of the plot as  $a$  approaches  $R_*$ .

Figure 1 shows that tidal heating of a sunlike star by even a massive  $10 M_J$  planet does not significantly affect the stellar structure before the merger, and therefore was likely unobservable at the time of the archival image (12 yr before the merger). The tidal heating of the star could be observable if the heated region is closer to the surface ( $M_{\text{heat}} \ll 2 \times 10^{-2} M_\odot$ ) because  $\tau_{\text{tide}}/\tau_{\text{heat}} \propto M_{\text{heat}}^{-1}$ . In Section 5 we will argue that a qualitatively similar process—the transfer of orbital energy from the orbit into the outermost layers of the star—is responsible for the transient.

### 3.3. Planetary structure

As the orbital separation decreases, the planet experiences increased irradiation and tidal forces. Irradiation might inflate the planet (J. D. Hartman et al. 2016; T. D. Komacek & A. N. Youdin 2017; D. P. Thorngren et al. 2021); if 1% of the stellar flux reaches the center of the planet as heat, a warm Jupiter could expand in radius by up to a factor of a few as its star evolves off the main sequence (E. D. Lopez & J. J. Fortney 2016). This expansion would make the planet more vulnerable to photoevaporation (e.g., R. A. Murray-Clay et al. 2009) and tidal disruption.

Even if inflation is unimportant, the planetary mass-radius relation implies that some planets will overflow their Roche lobe above the surface of the star. If the mass transfer is stable, the orbit of the planet expands to a period roughly determined by the mass of the core of the planet (F. Valsecchi et al. 2014, 2015; B. Jackson et al. 2016), and subsequent tidal dissipation could again decrease the orbital separation. The combination of these



**Figure 1.** Tidal evolution tracks for a sunlike star with a  $10 M_J$  companion. The abscissa shows the ratio of the orbital decay time to the thermal time at the location of energy deposition (see equations 15 and 16); the ratio must be greater than unity for the deposited energy to be observable before the merger. The ordinate shows the ratio of the tidal luminosity to the intrinsic stellar luminosity (see equation 8); the ratio must be greater than unity for the tidal energy deposition to be significant. Each line corresponds to a different tidal quality factor. The squares mark the  $-12$  yr epoch at which the archival images of the progenitor were taken. When computing the thermal time, we assume energy is deposited in the outermost  $2 \times 10^{-2} M_\odot$  of the star. None of these tidal quality factors yield observable tidal heating before the merger (upper right region of the figure), suggesting that the archival image was unaffected by the star-planet interaction.

effects could play a significant role in shaping exoplanet populations (e.g., Y. A. Lazovik 2023; D. P. Thorngren et al. 2023). On the other hand, if mass transfer is unstable, the star tidally disrupts and accretes the planet (e.g., J. A. Faber et al. 2005; J. Guillochon et al. 2011; S.-F. Liu et al. 2013). Finally, if the planet is sufficiently dense, the planet can reach the stellar surface and fully merge with the star before being destroyed. This “merger” scenario is the focus of the following sections, although we briefly discuss tidal disruption in Section 5.4.1.

## 4. MERGER

### 4.1. Surface interaction

When the surface of the star and the planet come into contact, the former exerts a drag force on the latter, further dissipating orbital energy. Initially, only the surface region of the star is in contact with the planet, so we refer to this phase as the surface interaction. The strength of the drag force depends on the relative speed between the planet and the stellar surface. Before the merger,

tidal dissipation transfers angular momentum from the orbit of the planet to the star, increasing its rotation rate. If the orbital and stellar rotation frequencies are equal, the system is said to be in corotation. We can estimate the extent of corotation at the onset of the surface interaction by equating the change in orbital angular momentum to the change in the spin angular momentum of the star. The change in orbital angular momentum from an initial separation  $a_0$  to  $R_*$  is transferred to the star, i.e.,  $I_*\omega_{*,m} = M_p (a_0^2\omega_0 - R_*^2\omega_{\text{Kep},m})$ ,  $I_* = \eta M_* R_*^2$  is the moment of inertia of the star,  $\omega_{*,m}$  and  $\omega_{\text{Kep},m}$  are the stellar and Keplerian rotation frequencies at the onset of the merger, respectively, and  $a_0$  and  $\omega_0 = \sqrt{GM_*/a_0^3}$  are the initial separation of the planet and the orbital frequency at that separation, respectively. We find

$$\begin{aligned} \frac{\omega_{*,m}}{\omega_{\text{Kep},m}} &= \eta^{-1} \frac{M_p}{M_*} \left( \sqrt{\frac{a_0}{R_*}} - 1 \right) \\ &\approx 10^{-2} \left( \frac{\eta}{0.08} \right)^{-1} \left( \frac{M_p}{10^{-3} M_*} \right) \left( \sqrt{\frac{a_0}{R_*}} - 1 \right). \end{aligned} \quad (17)$$

The rotation periods of hot-Jupiter host stars are typically of order weeks (see Table 1 from [R. A. Tejada Arevalo et al. 2021](#)), much longer than the Keplerian orbital period at their surface. In that sense, these host stars rotate slowly, and their initial rotation rates are negligible. For a typical hot Jupiter with  $a_0 = 0.05 \text{ au} \approx 10 R_*$  this equation shows that the rotation rate at the onset of the surface interaction will be much smaller than the Keplerian one (see also [N. Soker & R. Tylenda 2006](#); [G. Privitera et al. 2016b](#)). We therefore approximate the relative speed between the planet and the stellar material as the Keplerian speed,

$$v_{\text{orb}} \approx \sqrt{GM_*/a} \quad (18)$$

The planet experiences drag as a result of both ram pressure and gravitational interactions with the stellar material. The ratio between these two drag forces is roughly the ratio between the geometrical ( $\pi R_p^2$ ) and gravitational ( $\pi R_a^2$ , where  $R_a \equiv 2GM_p/v_{\text{orb}}^2$ ) cross sections of the planet,

$$\begin{aligned} \left( \frac{R_p}{R_a} \right)^2 &\approx 3 \times 10^3 \left( \frac{M_*}{M_\odot} \right)^2 \left( \frac{M_p}{M_J} \right)^{-2} \left( \frac{R_p}{R_J} \right)^2 \\ &\times \left( \frac{a}{R_\odot} \right)^{-2}, \end{aligned} \quad (19)$$

For the star-planet combinations relevant to ZTF SLRN-2020, ram pressure drag dominates (see also Figure 2 from [R. Yarza et al. 2023](#)). The ratio between ram pressure drag and gravitational drag increases as the planet orbit decays because the orbital speed increases, shrinking the gravitational cross section. We therefore consider only ram pressure drag hereafter.

The magnitude of the drag force depends on the stratification of the stellar density profile; if the density scale height is much smaller than the size of the planet, its effective cross section is the area within roughly a scale height of its substellar point ([B. D. Metzger et al. 2012](#)). On the other hand, when the density scale height is much larger than the radius of the planet, the density is approximately constant across the surface of the planet, and the cross section of the planet is its standard geometrical cross section  $\pi R_p^2$ . We can quantify stratification using the number of density scale heights across a planet radius,  $\varepsilon_\rho \equiv R_p/H_\rho$ . When  $\varepsilon_\rho = 0$ , the density is constant, and when  $\varepsilon_\rho \gg 1$ , the density is strongly stratified on the scale of the planet. We will now estimate the properties of the star near its surface, including  $\varepsilon_\rho$ . We approximate the temperature near the surface as that of a thin adiabatic gas in hydrostatic equilibrium ([R. Yamazaki et al. 2017](#)),

$$\begin{aligned} T &\approx \frac{\gamma - 1}{\gamma} \frac{gz\mu}{k} \\ &\approx 5.5 \times 10^4 \text{ K} \left( \frac{M_*}{M_\odot} \right) \left( \frac{R_*}{R_\odot} \right)^{-2} \left( \frac{z}{10^{-2} R_\odot} \right), \end{aligned} \quad (20)$$

where

$$z \equiv R_* - a \quad (21)$$

is the depth,  $g = GM_*/R_*^2$  is the gravitational acceleration,  $k$  is the Boltzmann constant,  $\mu$  is the mean molecular weight (we used that of a fully ionized gas with hydrogen and metal mass fractions 0.74 and 0.02, respectively) and  $\gamma \approx 5/3$  is the adiabatic index. The scale height is  $H_\rho \approx c_s^2/g$ , where

$$\begin{aligned} c_s &= \sqrt{\frac{\gamma k T}{\mu}} \approx \sqrt{\frac{\gamma - 1}{\gamma} \frac{z}{R_*} \frac{GM_*}{R_*}} \\ &\approx 2.8 \times 10^6 \text{ cm s}^{-1} \left( \frac{M_*}{M_\odot} \right)^{1/2} \left( \frac{R_*}{R_\odot} \right)^{-1} \\ &\times \left( \frac{z}{10^{-2} R_\odot} \right)^{1/2} \end{aligned} \quad (22)$$

is the speed of sound. We find

$$H_\rho \approx \frac{\gamma - 1}{\gamma} z \approx 4 \times 10^{-3} R_\odot \left( \frac{z}{10^{-2} R_\odot} \right), \quad (23)$$

$$\varepsilon_\rho \equiv \frac{R_p}{H_\rho} \approx \frac{\gamma}{\gamma - 1} \frac{R_p}{z} \approx 25 \left( \frac{R_p}{R_J} \right) \left( \frac{z}{10^{-2} R_\odot} \right)^{-1}. \quad (24)$$

These estimates show that the stellar density is strongly stratified during the surface interaction. In Appendix A we derive the cross section of the planet as a function of  $\varepsilon_\rho$  (see also [B. D. Metzger et al. 2012](#)). The drag force is

$$F_d \approx \rho v_{\text{orb}}^2 \sigma \simeq \sqrt{2\pi} \rho v_{\text{orb}}^2 H_\rho^{3/2} R_p^{1/2}, \quad (25)$$

where  $\rho$  is the density at the substellar point of the planet, and  $\sigma \simeq \sqrt{2\pi} H_\rho^{3/2} R_p^{1/2}$  is the cross section of the

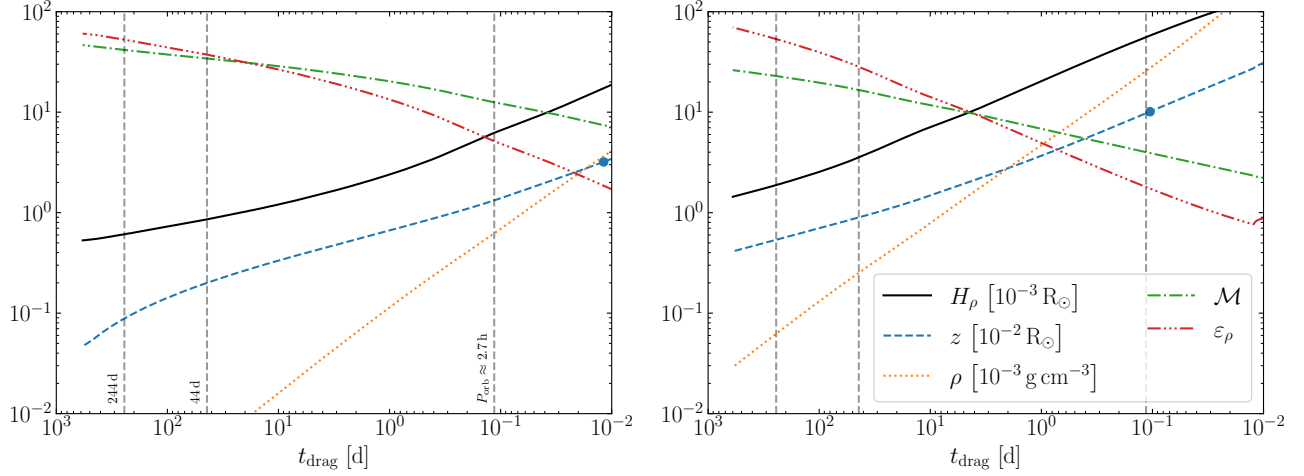


**Figure 2.** Important quantities during the merger between a sunlike star and a Neptune ( $15 M_{\oplus}$ ,  $3.5 R_{\oplus}$ , left panel) or a giant planet ( $10 M_J$ ,  $1 R_J$ , right panel), as a function of the timescale of orbital decay as a result of drag. Vertical dashed lines show the two epochs at which pre-merger constraints exist, as well as the orbital period at the surface of the star. The plots show the Mach number of the planet  $\mathcal{M} \equiv v_{\text{orb}}/c_s$ ,  $\varepsilon_\rho \equiv$  number of density scale heights across the planet, the depth  $z \equiv R_\star - r$  (with a circle indicating the location where the depth equals twice the radius of the planet), the stellar density  $\rho$ , and the density scale height  $H_\rho$ . The motion of the planet is always supersonic, leading to shocks. During the surface interaction, the flow is strongly stratified at the scale of the planet ( $\varepsilon_\rho > 1$ ).

planet in the  $\varepsilon_\rho \gg 1$  limit. Given this drag force, the characteristic timescale of orbital decay is

$$\begin{aligned} \tau_{\text{drag}} \approx \frac{H_\rho}{a} \frac{E_{\text{orb}}}{\dot{E}_{\text{drag}}} &= 16 \text{ h} \left( \frac{M_p}{M_J} \right) \left( \frac{\rho}{10^{-3} \text{ g cm}^{-3}} \right)^{-1} \\ &\times \left( \frac{R_\star}{R_\odot} \right)^{-1/2} \left( \frac{H_\rho}{10^{-2} R_\odot} \right)^{-1/2} \\ &\times \left( \frac{R_p}{R_J} \right)^{-1/2} \left( \frac{M_\star}{M_\odot} \right)^{-1/2}, \end{aligned} \quad (26)$$

where  $\dot{E}_{\text{drag}} = F_d v_{\text{orb}}$  is the rate of energy dissipation as a result of drag, and the factor of  $H_\rho/a$  accounts for the fact that the orbit need only decay by approximately a scale height for the drag to increase significantly. When the star and the planet just come into contact ( $a < R_\star + R_p$ ), the density is so low ( $\rho \ll 10^{-3} \text{ g cm}^{-3}$ ) that tides will still dominate. The timescale of orbital decay from tides near the surface is

$$\begin{aligned} \left( \frac{H_\rho}{a} \right) \tau_{\text{tide}} \Big|_{a=R_\star} &= \frac{4Q'_\star}{117} \frac{H_\rho}{R_\star} \frac{M_\star}{M_p} \sqrt{\frac{R_\star^3}{GM_\star}} \\ &\approx 18 \text{ yr} \left( \frac{H_\rho}{10^{-2} R_\star} \right) \left( \frac{Q'_\star}{10^6} \right) \\ &\times \left( \frac{M_\star}{M_\odot} \right)^{1/2} \left( \frac{M_p}{M_J} \right)^{-1} \\ &\times \left( \frac{R_\star}{R_\odot} \right)^{3/2}, \end{aligned} \quad (27)$$

where we used equation (10) for the tidal decay timescale. The factor of  $H_\rho/a$  appears for the same reason as in

equation (26). Equation (27) implies that for low quality factors or high planet masses, the orbital decay timescale at the surface could be months, and that the star and planet might not be in contact at the  $-244 \text{ d}$  epoch. If we instead assume the [K. Penev et al. \(2018\)](#) tidal quality factor, then, regardless of planet mass, tides are so inefficient at short orbital periods that drag dominates during the observed pre-merger epochs. Given the uncertainty in the tidal quality factor, and the difficulty in quantifying the drag-tides interaction without detailed models of the evolution of the stellar atmosphere, we assume drag dominate the orbital evolution once the star and planet come into contact, and use equation (26) as an estimate of the timescale of orbital decay.

Figure 2 shows important quantities as a function of the drag decay time, equation (26). We computed these quantities using the MESA stellar model (which we described in Section 2.1); the analytical estimates from the previous section give similar values. The left and right panels correspond to a Neptune and a gas giant, respectively. For most of the surface interaction, the orbital separation changes by a fractionally small amount (i.e.,  $a \approx R_\star$ ), so the orbital period is approximately equal to the orbital period at the stellar surface, which we show as a vertical dashed line. A blue line shows the depth of the planet within the envelope, with a blue dot showing when the planet becomes fully immersed. The orbital decay becomes dynamical (i.e.,  $\tau_{\text{drag}} = P_{\text{orb}}$ ) during the surface interaction (i.e., when  $z \lesssim 2R_p$ ), at which point the planet plunges into the stellar interior. The stellar density is strongly stratified (red line,  $\varepsilon_\rho \gtrsim 1$ ). We will

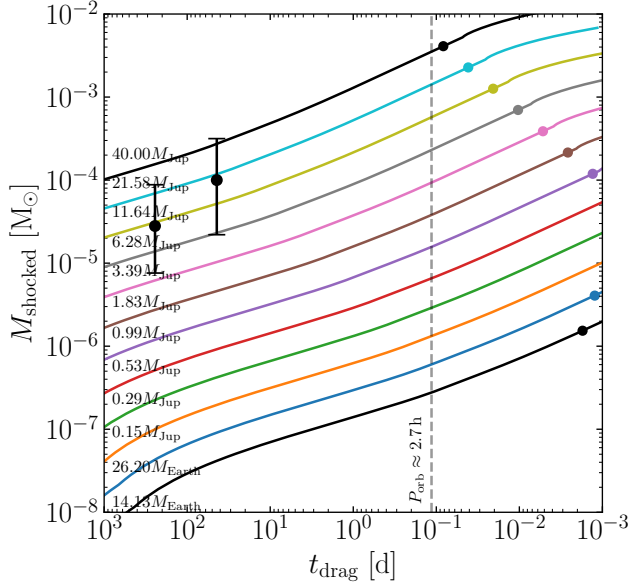


**Figure 3.** Mass shocked by the planet as a function of the drag decay time, for different planet masses. Dots show the point at which the planet is fully immersed. A dashed vertical line shows the orbital period of the planet when the orbital separation equals the stellar radius. Black error bars show constraints for the ejecta mass at two pre-merger epochs. These constraints suggest a planet with  $M_p \gtrsim 5 M_J$  satisfy these constraints.

discuss the other quantities shown in the figure when we discuss the physical processes to which they are relevant.

#### 4.2. Ejecta

We can use equation (22) to estimate the Mach number of the motion of the planet in the star,

$$\mathcal{M} \equiv \frac{v_{\text{orb}}}{c_s} \approx \sqrt{\frac{\gamma}{\gamma - 1} \frac{R_\star}{z}} \approx 16 \left( \frac{z}{10^{-2} R_\odot} \right)^{-1/2} \left( \frac{R_\star}{R_\odot} \right)^{1/2}. \quad (28)$$

Figure 2 shows the Mach number computed using the stellar model, which agrees with the prediction from equation (28) that the motion of the planet is always supersonic ( $\mathcal{M} > 1$ ). Therefore, the planet will shock the stellar material. The observational consequences of these shocks depend on the location of the shocked material. If the material is close to the surface (e.g., during the surface interaction), the shocked material can form an outflow and escape without significant confinement from stellar material above it. In contrast, if the shocked material is deep in the interior (e.g., once the planet is fully immersed), the energy of the shocks will be shared with the layers closer to the surface, and the planet can be more reasonably approximated as a heat source in the stellar interior. While the details of ejecta formation

depend on the hydrodynamics of the interaction, we use full immersion as the approximate condition at which the efficiency of ejecta formation decreases significantly.

The energy deposited close to the surface can escape more easily, so it is observable on shorter timescales. This near-surface energy deposition can more easily produce ejecta either dynamically or as a wind, depending on the duration, amplitude, and depth of the energy deposition. The energy deposited deeper in the star is likely to escape only on the longer Kelvin–Helmholtz time of the envelope, and might not be observable on the timescale of the ZTF SLRN-2020 transient. For this reason, we argue that the surface interaction is responsible for the transient (see also [N. Soker & R. Tytenda 2006](#)).

The change in orbital energy as the orbit of the planet decays from  $a = R_\star$  to  $a = R_\star - z$  is

$$\begin{aligned} \Delta E_{\text{orb}} &\approx \left. \frac{dE_{\text{orb}}}{da} \right|_{a=R_\star} z = E_{\text{orb}} z / R_\star, \\ &= 1.86 \times 10^{44} \text{ erg} \left( \frac{M_p}{M_J} \right) \left( \frac{M_\star}{M_\odot} \right) \left( \frac{z}{R_J} \right) \\ &\quad \times \left( \frac{R_\star}{R_\odot} \right)^{-2}, \end{aligned} \quad (29)$$

where we let  $a \approx R_\star$ . The planet will impart an average specific energy of order  $v_{\text{orb}}^2$  on the shocked material. We can estimate the amount of mass that is shocked during the surface interaction as

$$\begin{aligned} M_{\text{shocked}} &\approx \Delta E_{\text{orb}} / v_{\text{orb}}^2 = \frac{1}{2} M_p \frac{z}{R_\star} \\ &\approx 4.9 \times 10^{-5} M_\odot \left( \frac{M_p}{M_J} \right) \left( \frac{z}{R_J} \right) \left( \frac{R_\star}{R_\odot} \right)^{-1}. \end{aligned} \quad (30)$$

A fraction of this shocked mass will become unbound. The shocked mass is much smaller than the mass of the planet because during the surface interaction the planet transfers into the envelope only a fraction  $R_p/R_\star \approx 0.1 (R_p/R_J) (R_\star/R_\odot)^{-1} \ll 1$  of its orbital energy. If we assume that the efficiency of mass ejection decreases significantly when the planet becomes fully immersed, then we can estimate the total shocked mass by setting  $z = 2R_p$  and invert equation (30) to find the minimum planet mass required to produce a given amount of ejecta,

$$\begin{aligned} M_p &> M_{\text{ej}} \frac{R_\star}{R_p} \\ &= 1 M_J \left( \frac{M_{\text{ej}}}{10^{-4} M_\odot} \right) \left( \frac{R_\star}{R_\odot} \right) \left( \frac{R_p}{R_J} \right)^{-1} \end{aligned} \quad (31)$$

Figure 3 shows the shocked mass as a function of the drag decay time for planets of different masses. The black error bars show estimates of the pre-merger ejecta mass ([K. De et al. 2023](#)). The vertical dashed line shows the orbital period at the surface of the star; the orbital

decay becomes dynamical at that point. Circles show the point at which the planet is fully immersed in the star (i.e.,  $z = 2R_p$ ). The plot shows that a massive planet ( $M_p \gtrsim 5M_J$ ) is most consistent with the observations. We will examine the constraints on the planet mass in more detail in Section 6.

We have made several approximations in the arguments above and Figure 3. The first one is the omission of tides, which we discussed in Section 4.1; if tides are important, then, at a given depth, drag is responsible for only a fraction of the dissipated orbital energy, and the corresponding shocked mass is smaller than if tides were negligible. The second is that we have not modeled the hydrodynamical interaction between the planet and the star. Finally, when plotting the observational constraints in Figure 3, we have effectively assumed that the ejecta travels instantly to the dust condensation radius  $R_{\text{dust}}$ ; in reality, the ejecta forming the dust must have been produced a time  $\approx \sqrt{R_{\text{dust}}^3/GM_\star}$  before the dust observation. The goal of this section has been to estimate the amount of energy available during the surface interaction; these estimates show that, if shocks during the surface interaction are the dominant mechanism producing ejecta, then only massive planets are consistent with the pre-merger observations.

#### 4.3. Destruction of the planet

The planet experiences tidal forces and ram pressure in the star. These processes eventually destroy the planet. The evolution of the internal structure of the planet during the merger is uncertain, but is often estimated from order-of-magnitude arguments. The star tidally disrupts the planet approximately when the average densities of the planet and the mass enclosed by its orbit are equal. The ram pressure of the stellar gas disrupts the planet approximately when it equals the average binding energy per unit volume of the planet (S. Jia & H. C. Spruit 2018), i.e.,

$$\rho v_{\text{orb}}^2 = \bar{\rho}_p v_{\text{esc,p}}^2, \quad (32)$$

where  $\bar{\rho}_p$  is the average density of the planet and  $v_{\text{esc,p}} = (2GM_p/R_p)^{1/2}$  is the escape speed from its surface.

Hydrodynamical simulations suggest that the planet gradually loses mass to hydrodynamical ablation in the stellar envelope (e.g., S. D. Murray et al. 1993; E. Sandquist et al. 1998; J.-C. Passy et al. 2012; M. Y. M. Lau et al. 2025). The energetics of the debris is unclear; it can transfer some of its kinetic energy into the envelope, but it also gains thermal energy from the envelope because it is much colder (see section 3.4 in C. E. O'Connor et al. 2023). Given the uncertainties associated with these processes, we only note that the conditions for the destruction of both planets we consider in Figure 2 are met only once they are fully immersed.

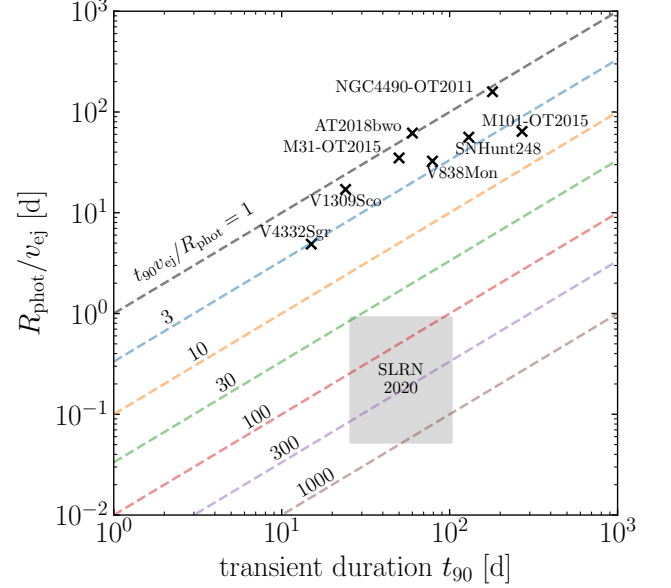


**Figure 4.** Comparison between the time needed for ejecta at speed  $v_{\text{ej}}$  to reach the observed photosphere ( $R_{\text{phot}}/v_{\text{ej}}$ ) and the duration of the transient  $t_{90}$  (defined as the time since peak at which 90% of the total radiated energy has been radiated). Scatter points show the observed properties of several stellar mergers. For most of them, these two timescales are within a factor of a few from each other. ZTF SLRN-2020 lies somewhere in the shaded region, depending on the definition of the duration of the transient (only the plateau  $\approx 25$  d or the full light curve  $\approx 100$  d) and on the assumed speed of the ejecta (ranging from the speed of the expanding inner dust shell  $\approx 35 \text{ km s}^{-1}$  to the escape velocity from a sunlike star  $\approx 618 \text{ km s}^{-1}$ ). The duration of ZTF SLRN-2020 is much longer than the time it would take ejecta to reach the observed photosphere, so it is likely not powered by hydrogen recombination from a single episode of mass ejection.

## 5. THE ZTF SLRN-2020 TRANSIENT

### 5.1. Comparison to luminous red novae

It is helpful to compare ZTF SLRN-2020 to LRNe, a transient class associated with stellar (i.e., star-star) mergers (R. Tytenda et al. 2011; N. Ivanova et al. 2013). Stellar and star-planet mergers have qualitatively similar light curves (see the top panel of Figure 2c of K. De et al. 2023, for a comparison between the light curves of ZTF SLRN-2020 and a few LRNe). These similarities motivate studying whether the same physical processes are responsible for producing their light curves and, more broadly, the extent to which star-planet mergers are “scaled-down” stellar mergers.

We begin by briefly summarizing the physical processes responsible for luminous red novae (LRNe) light curves. When the companion plunges into the stellar interior, it produces ejecta on a timescale comparable to the orbital period (M. MacLeod et al. 2018b). This ejecta

has a distribution of speeds centered around  $\approx v_{\text{orb}}$  (see, e.g., Figure 5 from T. Hutchinson-Smith et al. 2024). This ejecta produces a light curve with two phases (M. MacLeod et al. 2017; T. Matsumoto & B. D. Metzger 2022): (i) an initial peak, corresponding to the thermal emission of the high-velocity, low-mass “tail” of the ejecta energy distribution, and (ii) a longer plateau caused by the recombination of hydrogen in the bulk of the ejecta. The ejecta expands and cools until reaching the recombination temperature of hydrogen,  $\approx 10^4$  K. The radius at which the hydrogen recombines is approximately the radius of the photosphere because the opacity of atomic hydrogen is much smaller than that of ionized hydrogen.

The recombination radius is at least a factor of a few larger than the radius of the star, so ejecta must move at a significant fraction of the escape speed to reach the recombination radius. The slowest component of the ejecta to significantly contribute to the recombination transient therefore has speed  $\approx v_{\text{esc}}$ . Therefore, the duration of the transient is roughly the time it takes for this marginally unbound component of the ejecta to reach the recombination radius, i.e.,  $\approx R_{\text{phot}}/v_{\text{esc}}$ . The actual speed of the ejecta  $v_{\text{ej}}$  might be different from  $v_{\text{esc}}$  depending on, e.g., the radius at which the ejecta is launched and the post-ejection evolution. Figure 2 from T. Matsumoto & B. D. Metzger (2022) shows that, for stellar mergers involving stars of roughly similar mass to ZTF SLRN-2020, the observed ejecta speed is within a factor of a few from the surface escape speed of the star.

Figure 4 shows  $t_{90}$  (defined as the time since peak at which 90% of the total radiated energy has been radiated) and  $R_{\text{phot}}/v_{\text{ej}}$  for a subset of known LRNe and for ZTF SLRN-2020. These two timescales are within a factor of a few for all LRNe, in agreement with our rough estimate of the transient duration outlined above. We also show a shaded region for ZTF SLRN-2020, accounting for uncertainties in the ejecta velocity and on the definition of transient duration appropriate in this context. As a lower limit for the speed, we use the expansion velocity of the inner radius of the dust shell  $v_{\text{ej}} \approx 35 \text{ km s}^{-1}$ , as determined from the SED at 120 d and 320 d (Section 2.3 and K. De et al. 2023). As an upper limit, we use the escape speed from the surface of the star,

$$v_{\text{esc}} = 618 \text{ km s}^{-1} (M_{\star}/M_{\odot})^{1/2} (R_{\star}/R_{\odot})^{-1/2}. \quad (33)$$

The two limits for the duration of the transient are the duration of the plateau ( $\approx 25$  d) and of the entire light curve ( $\approx 100$  d).

The figure shows that the duration of ZTF SLRN-2020 is much longer than  $R_{\text{phot}}/v_{\text{ej}}$ . If the light curve were produced by the recombination of dynamically produced ejecta, the duration of the transient would be between

$$\frac{R_{\text{phot}}}{v_{\text{esc}}} = 1 \text{ h} \left( \frac{R_{\text{phot}}}{3.5 R_{\odot}} \right) \left( \frac{M_{\star}}{M_{\odot}} \right)^{-1/2} \left( \frac{R_{\star}}{R_{\odot}} \right)^{1/2} \quad (34)$$

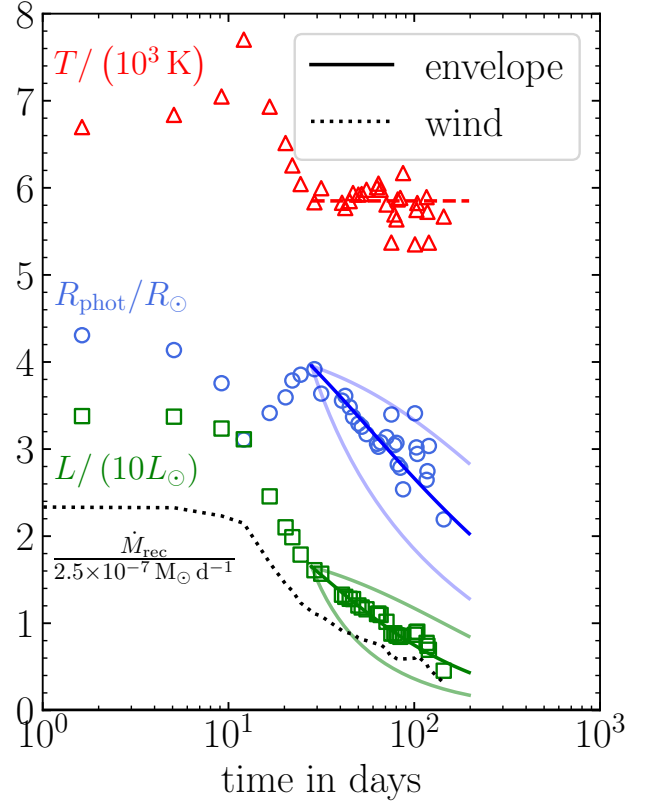


**Figure 5.** Bolometric properties of ZTF SLRN-2020 as a function of time. Hollow points show the observations (K. De et al. 2023). Solid opaque lines show a model of a contracting envelope of mass  $1.1 \times 10^{-6} M_{\odot}$  around the merger remnant; semi-transparent lines show models with masses three times as small or as large. The horizontal dashed line is the constant effective temperature (5850 K) assumed in the envelope model. A dotted line shows the approximate required mass loss rate if the light curve were powered by the recombination of hydrogen in an outflow.

and

$$\frac{R_{\text{phot}}}{35 \text{ km s}^{-1}} \approx 0.8 \text{ d} \left( \frac{R_{\text{phot}}}{3.5 R_{\odot}} \right), \quad (35)$$

which is much shorter than the full duration of  $\approx 100$  d. Other work arrived at similar estimates for the transient duration (e.g., equation (22) from R. Yamazaki et al. 2017). We conclude that a single mass ejection episode cannot account for the full duration of the ZTF SLRN-2020 light curve.

## 5.2. Powering mechanism

The hollow points in Figure 5 show the bolometric properties of ZTF SLRN-2020 as a function of time with respect to the optical peak (K. De et al. 2023, see Section 2.3 for a summary of how they derived these properties). The light curve has at least two components. First, a plateau in all properties at times  $t \lesssim 10$  d, at the

end of which the photosphere cools and shrinks. There is a transition around  $\approx 12$  d at which the photosphere heats and expands again, reaching a local maximum of  $\approx 4 R_\odot$  at  $\approx 25$  d. After that, it gradually contracts at constant effective temperature, with the scatter in the photometric properties increasing drastically after  $\approx 70$  d as the transient dims. Here we examine the decay at times  $> 25$  d, where most of the energy is radiated.

A possible powering mechanism is the recombination of hydrogen in an outflow driven by the energy deposition from the planet. After the planet plunges into the interior, the energy deposition at increasing depths becomes increasingly inefficient at driving an outflow, so the mass loss rate decreases with time. The required mass loss rate to explain the luminosity is approximately

$$\dot{M}_{\text{rec}} = \frac{m_p}{X E_H} L, \quad (36)$$

where  $E_H = 13.6$  eV is the ionization energy of hydrogen,  $X \approx 0.74$  is the mass fraction of hydrogen, and  $m_p$  is the mass of the proton. The dashed black line in Figure 5 shows the mass loss rate required to explain the light curve entirely via recombination of hydrogen. Since the luminosity of the outflow is proportional to the wind mass loss rate, the implied mass loss rate is  $\dot{M}_{\text{rec}} \propto L \propto t^{-0.7}$  at late times. The total ejecta mass, assuming hydrogen recombination powers the entire (initial plateau and subsequent decay) of the light curve, is  $\approx 3 \times 10^{-5} M_\odot$ .

We will now examine a different possible powering mechanism for this part of the light curve. During the surface interaction, the shocks from the planet will impart the ejecta with a distribution of energies. A fraction of the ejecta will remain bound, forming an extended envelope that contracts over the course of its Kelvin–Helmholtz time. During this contraction, the envelope radiates the energy that the planet deposited, producing a transient.

Several LRNe show emission consistent with a contracting envelope. After their main outbursts, the luminosity and photosphere radius of V838 Mon and V4332 Sag decreased over several years in a manner consistent with a contracting envelope (see figures 4 and 2, respectively, from R. Tylenda et al. 2005; R. Tylenda 2005). In those transients, however, mass ejection on a dynamical timescale powers the light curve on timescales of weeks to months, and the evolution of the material that remains bound to the star dominates the light curve only on timescales of years. Based on a similar comparison to LRNe, E. Bear et al. (2011) proposed that a contracting envelope would be responsible for the late-time light curve during a merger between a brown dwarf and a planet. We will now determine whether a contracting envelope can reproduce the ZTF SLRN-2020 light curve.

We review this model, as presented in R. Tylenda et al. (2005), in Appendix B, and discuss its main properties here. We assume that, as a result of the energy deposition, the star forms an extended envelope whose

structure can be described as a polytrope with polytropic index  $n = 3/2$ . As the envelope contracts, it loses energy. The rate of change of the energy of the envelope—which is related to the rate of change of its radius—is equal in magnitude to its luminosity. This equality results in a differential equation for the envelope radius as a function of time. We assume a constant representative temperature of 5850 K throughout the contraction (shown as a red horizontal dashed line in Figure 5). The solid lines in Figure 5 show a model of a contracting envelope around a sunlike star. The envelope contracts appreciably on its Kelvin–Helmholtz timescale,

$$\begin{aligned} t_{\text{KH}} &= \frac{GM_{\text{env}}M_\star}{2R_{\text{env}}L_{\text{env}}} \\ &= 40 \text{ d} \left( \frac{M_{\text{env}}}{10^{-6} M_\odot} \right) \left( \frac{M_\star}{M_\odot} \right) \left( \frac{R_{\text{env}}}{5 R_\odot} \right)^{-1} \\ &\quad \times \left( \frac{L_{\text{env}}}{10^{35} \text{ erg s}^{-1}} \right)^{-1}, \end{aligned} \quad (37)$$

We set the initial radius and luminosity of the envelope to the observed values and choose the mass of the envelope such that the contraction timescale of the envelope matches the observations. That envelope mass is  $M_{\text{env}} = 1.1 \times 10^{-6} M_\odot$ . We also show for comparison envelopes three times less and more massive. The contracting envelope model can reasonably reproduce the late-time  $\propto t^{-0.7}$  decay of the light curve.

In reality, both of these powering mechanisms likely play a role, with some of the shocked material becoming unbound and forming a recombination wind, and some of the material remaining bound and forming a contracting envelope.

### 5.3. Future evolution

On timescales longer than the initial transient, any energy deposited deeper in the star becomes the dominant perturbation to the intrinsic stellar luminosity (B. D. Metzger et al. 2012). The deeper the energy deposition, the longer it will take to reach the surface. The star will return to its original state only on the much longer Kelvin–Helmholtz time of the deepest heated region. Therefore, follow-up observations could constrain the properties of the heating. For example, if the star returns to its pre-merger luminosity on timescales much shorter than its global Kelvin–Helmholtz time, it would rule out a large thermal perturbation deep in the star.

The exact association between the timescale over which the star returns to its unperturbed state and the properties of the planet is less straightforward. In principle, more resilient planets could heat deeper regions of the star (although the details depend on the dynamical and energetic distribution of the planetary debris). Although a less massive but denser planet will survive deeper in the star, the luminosity perturbation from the cooling of the deeper layers might be so small—because the planet

is small—that the perturbed luminosity becomes observationally indistinguishable from the unperturbed one much sooner than the Kelvin–Helmholtz time of the deepest heated region. B. D. Metzger et al. (2017) considered a star-planet merger as a potential explanation for the secular dimming of KIC 8462852 (T. S. Boyajian et al. 2016), an F-type main-sequence star. They used a one-dimensional stellar evolution code to model the evolution of the star following heating by a merger with companions ranging from Io to a  $50 M_J$  brown dwarf. The star took roughly a hundred times longer to return to its original luminosity if the companion was a brown dwarf rather than a Jupiter. However, even though the Earth survived deeper than the Jupiter because it is denser (they considered only destruction via tidal disruption), its orbital energy is so much smaller that the luminosity of the star became similar to the unperturbed luminosity sooner than for the Jupiter (see Figures 1 and 2 from B. D. Metzger et al. 2017).

During the merger, the planet also deposits its angular momentum into the star. Therefore, as a result of angular momentum conservation after the merger, another prediction of the contracting envelope model is that the surface rotation rate of the star should increase as  $R_{\text{phot}}^{-2}$ . However, the dusty obscuration of the photosphere in the K. De et al. (2023) spectra makes the rotation rate shortly after the merger uncertain.

#### 5.4. Alternative scenarios

##### 5.4.1. Tidal disruption event

Another possible outcome of the star-planet interaction is the tidal disruption of the planet above the stellar surface. E. Bear & N. Soker (2011) and B. D. Metzger et al. (2012) studied the transients arising from the tidal disruption of a planet by a brown dwarf and a star, respectively. Qualitatively, the evolution is as follows (B. D. Metzger et al. 2012): the debris of the disrupted planet forms a disk around the star. The accretion rate is higher than the Eddington accretion rate, resulting in an outflow with a characteristic luminosity

$$L \approx 10^{37} \text{ erg s}^{-1} (M_p/M_J). \quad (38)$$

Once the accretion rate is below the Eddington rate, which occurs after a time  $\approx t_{\text{Edd}} \approx 80 \text{ d} (M_p/M_J)^{3/4}$ , the emission from the accretion disk becomes directly visible. At that point, the transient becomes brighter and hotter, since the effective temperature in the disk at radial coordinate  $r$  is (see equation (29) from B. D. Metzger et al. 2012)

$$T_{\text{acc}} \approx 6.6 \times 10^4 \text{ K} \left( \frac{\dot{M}}{\dot{M}_{\text{Edd}}} \right)^{1/4} \left( \frac{r}{R_\odot} \right)^{-3/4}. \quad (39)$$

In ZTF SLRN-2020, however, the effective temperature remains  $\lesssim 10^4 \text{ K}$  throughout the transient (Figure 5

and K. De et al. 2023), suggesting that the emission is not arising from a hot accretion disk. If we instead let  $t_{\text{Edd}} > 100 \text{ d}$  (by setting  $M_p \gtrsim M_J$ ), so that the observed transient is a result of the super-Eddington wind (before the disk becomes visible), the luminosity of that wind (equation (38),  $\gtrsim 10^{37} \text{ erg s}^{-1}$ ) would be much larger than the observed one ( $\approx 10^{35} \text{ erg s}^{-1}$ ). We therefore consider it unlikely that ZTF SLRN-2020 is a planetary tidal disruption event.

##### 5.4.2. Jet formation

Jets are a potential powering mechanism for merger transients (e.g., N. Soker 2020; N. Soker & N. Kaplan 2021). N. Soker (2023) studied the potential role on jets in ZTF SLRN-2020, and suggested that the planet could have accreted material from the star during the pre-merger epochs and launched a jet. To allow accretion, the relative velocity between the stellar surface and the planet must be smaller than we have assumed; in particular, it must be much smaller than the orbital velocity, so that gravitational capture can form an accretion disk around the planet. In this scenario, the terminal velocity of jet ejecta is approximately the escape speed from the object launching the jet. Since, for a planet  $\approx 10 M_J$ , the escape velocity of the planet and of the star are of the same order, some jet material might become unbound but have a small terminal speed. N. Soker (2023) suggested that this process could explain the  $\approx 35 \text{ km s}^{-1}$  expansion speed of the inner edge of the dust shell (Section 2.3 and K. De et al. 2023). A prediction from this scenario is that ZTF SLRN-2020 will form a bipolar nebula.

##### 5.4.3. Accretion outburst onto a young stellar object

K. De et al. (2023) considered the possibility that ZTF SLRN-2020 was the result of an accretion episode onto a young stellar object (YSO; for a review on accretion onto young stars, see L. Hartmann et al. 2016). They found it unlikely because the optical and near-IR spectra lacked the atomic emission lines characteristic of hot accreting gas. The estimated evolutionary stage of the ZTF SLRN-2020 star (on or slightly beyond the main sequence) sets it apart from two other star-planet merger candidates: ASASSN-15qi (G. J. Herczeg et al. 2016; A. Kashi & N. Soker 2017) and ASASSN-13db (A. Sicilia-Aguilar et al. 2017; A. Kashi 2018; A. Kashi et al. 2019). The stars in those transients are YSOs, and they experienced other outbursts within decades of the potential star-planet outburst. The possibility of accretion outbursts in those two sources makes the unambiguous determination of the cause of a particular outburst more challenging.

## 6. ENERGETIC CONSTRAINTS

We will now combine the results of previous sections with the observed energetic properties of ZTF SLRN-2020. The orbital energy of the planet powers the transient, so the energetics can constrain the mass of the

planet. We will consider the constraints from both the pre-merger observations and from the light curve during the main transient.

### 6.1. From the pre-merger observations

There are observational constraints of the ejecta mass at three epochs. We summarized those constraints in Section 2. The energy required to produce ejecta is

$$E_{\text{ej}} = \frac{1}{2} M_{\text{ej}} v_{\text{esc}}^2 \approx 3.79 \times 10^{44} \text{ erg} \left( \frac{M_{\text{ej}}}{10^{-4} M_{\odot}} \right) \left( \frac{M_{\star}}{M_{\odot}} \right) \left( \frac{R_{\star}}{R_{\odot}} \right)^{-1}, \quad (40)$$

In Section 4.2 we studied the scenario in which the pre-merger ejecta is produced as the planet interacts with the stellar surface. Figure 3 shows the mass that the planet has shocked as a function of epoch, for planets of different masses. Given the small fraction of the orbital energy that is available in the small change in orbital separation between the two epochs, this mechanism requires a massive planet. In that section, we estimated that planets with masses

$$M_{\text{p}} \gtrsim 5 M_{\text{J}} \quad (41)$$

are necessary to meet the pre-merger ejecta constraints. K. De et al. (2023) arrived at a similar estimate  $M_{\text{p}} \approx 10 M_{\text{J}}$  by extrapolating models of pre-merger mass loss in stellar mergers (M. MacLeod & A. Loeb 2020).

### 6.2. From the main outburst

The radiated energy during the transient is  $6.5 \times 10^{41}$  erg. Constraining the orbital energy from the radiated energy requires the radiative efficiency, which can vary by orders of magnitude depending on the process responsible for the radiation. For example, consider the recombination wind and the contracting envelope we discussed in Section 5. The energy radiated by the contracting envelope is equal to the energy it took to inflate it, so the radiative efficiency is unity. In contrast, to form a recombination wind, the gas in the wind must be effectively unbound. The energy released by recombination is only a fraction

$$\epsilon_{\text{rec}} = \frac{13.6 \text{ eV}}{m_{\text{p}} v_{\text{esc}}^2} \approx 3 \times 10^{-3} \quad (42)$$

of the energy required to unbind the gas, so the radiative efficiency is smaller.

If the entire light curve is the result of a recombination wind, the implied ejecta mass is

$$M_{\text{ej}} = \frac{E_{\text{rad}}}{E_{\text{H}}} \frac{m_{\text{p}}}{X} \approx 3.4 \times 10^{-5} M_{\odot}. \quad (43)$$

From equation 31 and the planet mass-radius relation the planet mass that corresponds to this amount of ejecta is

$$M_{\text{p}} \approx 0.3 M_{\text{J}}, \quad (44)$$

$$R_{\text{p}} \approx 1 R_{\text{J}}. \quad (45)$$

In contrast, if we assume a radiative efficiency of unity, the constraint on the planet mass follows from

$$\left. \frac{dE_{\text{orb}}}{da} \right|_{a=R_{\star}} z = E_{\text{rad}}, \quad (46)$$

yielding

$$M_{\text{p}} \approx 3.5 M_{\oplus}, \quad (47)$$

$$R_{\text{p}} \approx 1.7 R_{\oplus}, \quad (48)$$

where we set  $z = 2R_{\text{p}}$ .

The planet mass constraints in equations (44) and (47) are smaller than the pre-merger constraint from equation (41). This difference warrants further examination, as it is unclear whether the larger planetary masses we estimate from the pre-merger observations are consistent with the merger light curve. Figure 3 shows that the rate at which the planet shocks stellar material increases steeply as the orbital decay time decreases. A significant fraction of the total ejecta is likely produced in the last few orbital periods before the planet plunges into the stellar interior (B. D. Metzger et al. 2012; M. Y. M. Lau et al. 2025). The recombination transient associated with this mass ejection on dynamical timescales has a characteristic duration of hours (R. Yamazaki et al. 2017), which is shorter than the ZTF cadence of  $\approx$  days. It is therefore possible that a fraction of the ejecta of the transient was produced over a timescale inaccessible to ZTF.

While some dynamical ejecta might not appear in the transient light curve, it should eventually form dust, for which there are post-merger observational constraints. These dust constraints arise from the evolution of the SED, not from the light curve, so they are free from cadence effects. As we discussed in Section 2.3, K. De et al. (2023) and R. M. Lau et al. (2025) estimated the ejecta mass to be  $\approx 10^{-4} M_{\odot}$  (see equation (5)). This amount is slightly larger than required by a recombination wind (the least radiatively efficient mechanism we consider, equation (43)), supporting the idea that the light curve does not capture at least some dynamical mass ejection. The observed ejecta mass suggests that the electromagnetic signatures of only a fraction of the ejecta appear in the ZTF light curve, ranging from  $\approx$  a percent (in the cooling-envelope model) to  $\approx$  tens of percents (in the recombination wind model).

Equation (31) shows that a planet at least as massive as Jupiter is needed to produce the observed  $\approx 10^{-4} M_{\odot}$  of post-merger ejecta. The uncertainties in the lower end of the observed ejecta mass are significant, but the best-fit value of  $\approx 10^{-4} M_{\odot}$  energetically rules out a planet with mass between Earth and Neptune (e.g., equation 47). For this reason, we favor a planet at least as massive as Jupiter.

## 7. CONCLUSIONS

K. De et al. (2023) interpreted the ZTF SLRN-2020 transient as a star-planet merger. Here, we explored

this possibility in more detail through models of the system before and during the merger. We used the pre-merger dust formation observations to estimate the mass of the planet to be  $\gtrsim 5 M_J$ . We argued that the most promising mechanisms responsible for the light curve are the contraction of an inflated envelope around the merger remnant or the recombination of hydrogen in an outflow. We also argued that some of the ejecta was produced on a dynamical timescale and is unobservable in the ZTF light curve, but observable through post-merger dust formation. We summarize our results in more detail below.

The pre-merger evolution likely consists of a planet whose orbit decayed as a result of tidal dissipation. The archival image and the small photosphere radius during the transient support the idea that planets can merge with their host stars during the main sequence or early during the post-main-sequence. At the time of the archival image, the tidal interactions between the star and the planet had not affected the appearance of the star (Figure 1).

Once the star and the planet come into contact, drag forces affect the orbital decay of the planet. The planet shocks the stellar material at the surface, ejecting some of it. This mechanism can account for the pre-merger ejecta if the mass of the planet is  $\gtrsim 5 M_J$  (Figure 3). A planet in this mass range has a mean density of  $\gtrsim 5 M_J$ , much higher than the  $\approx 1 \text{ g cm}^{-3}$  of the roughly sunlike star in ZTF SLRN-2020. This density contrast is consistent with the planet avoiding tidal disruption above the stellar surface. Energy deposited deep in the stellar interior, if any, likely reaches the surface only on timescales longer than the duration of the transient.

The duration of the light curve suggests that ZTF SLRN-2020 cannot be powered by a single episode of mass ejection on a dynamical timescale (Figure 4). It is possible, however, that the planet ejected mass dynamically as it plunged into the stellar interior, as predicted by previous work (e.g., B. D. Metzger et al. 2012; R. Yamazaki et al. 2017; M. Y. M. Lau et al. 2025). The timescale of this dynamical transient  $\approx$  hours might be shorter than the cadence of the observations. The light curve can be the result of a recombination wind with a decreasing mass loss rate (requiring  $3.4 \times 10^{-5} M_\odot$  of outflow), or as the contraction of a remnant inflated envelope of  $\approx 10^{-6} M_\odot$ . Likely, both mechanisms play a role, with some shocked material becoming unbound and recombining, and some remaining bound and contracting gradually. The detection of circumstellar gas around the remnant (M. Y. M. Lau et al. 2025) indeed suggests that some shocked material remains bound.

Estimates of the ejecta mass at the 320 d epoch of  $\approx 10^{-4} M_\odot$ —larger than implied by a recombination wind—tentatively support the idea that some dynamical

mass loss is absent from the light curve. Energetically, the best-fit value for the mass of the observed post-merger ejecta suggests a planet at least as massive as Jupiter. Combined with the pre-merger ejecta constraints, the observed ejecta masses suggest ZTF SLRN-2020 was the result of a merger between a star and a planet with mass at least several times that of Jupiter. Future models combining hydrodynamics and radiative transfer could improve our understanding of these mergers and determine the properties of their progenitor systems.

## ACKNOWLEDGMENTS

We thank Elisabeth Adams, Andrea Antoni, Evan Bauer, Matteo Cantiello, Rosa Wallace Everson, Brian Jackson, Seth Jacobson, Ryan Lau, Abraham Loeb, Brian Metzger, Sarai Rankin, Melinda Soares-Furtado, Alexander Stephan, and Ashley Villar for discussions. We thank Kishalay De for discussions and for sharing the observation data in Figure 5. RY is grateful for support from a Doctoral Fellowship from the University of California Institute for Mexico and the United States (UCMEXUS), a Texas Advanced Computing Center (TACC) Frontera Computational Science Fellowship, and a NASA FINESST award. This research was possible thanks to funding at UC Santa Cruz through the Heising-Simons Foundation, NSF grants: AST 1852393, AST 2150255 and AST 2206243. M.M. gratefully acknowledges support from the Clay Postdoctoral Fellowship of the Smithsonian Astrophysical Observatory. B.I. acknowledges support from the University of California President’s Postdoctoral Fellowship (PPFP) and the Vera Rubin Postdoctoral Fellowship. This research has made use of NASA’s Astrophysics Data System Bibliographic Services.

*Software:* Mathematica, matplotlib (J. D. Hunter 2007), MESA r24.08.1 (G. M. Fuller et al. 1985; C. A. Iglesias & F. J. Rogers 1993; T. Oda et al. 1994; D. Saumon et al. 1995; C. A. Iglesias & F. J. Rogers 1996; N. Itoh et al. 1996; C. Angulo et al. 1999; K. Langanke & G. Martínez-Pinedo 2000; F. X. Timmes & F. D. Swesty 2000; F. J. Rogers & A. Nayfonov 2002; A. W. Irwin 2004; J. W. Ferguson et al. 2005; S. Cassisi et al. 2007; A. I. Chugunov et al. 2007; R. H. Cyburt et al. 2010; A. Y. Potekhin & G. Chabrier 2010; B. Paxton et al. 2011, 2013, 2015; J. Poutanen 2017; B. Paxton et al. 2018, 2019; S. Blouin et al. 2020; A. S. Jermyn et al. 2021, 2023), MESA SDK 24.7.1 (R. Townsend 2024), numpy (C. R. Harris et al. 2020), pandas (W. McKinney 2010), py\_mesa\_reader (J. Schwab et al. 2024), scipy (P. Virtanen et al. 2020), unyt (N. J. Goldbaum et al. 2018).

## APPENDIX

## A. RAM PRESSURE DRAG

We approximate the drag force as the integral the momentum flux over the cross section of the planet,

$$F = \int \rho v_{\text{orb}}^2 d\sigma. \quad (\text{A1})$$

Approximating the orbital speed as constant across the planet, and the density profile as exponential with a scale height at the substellar point  $H_\rho$ , we obtain

$$F_d = \rho v_{\text{orb}}^2 \sigma, \quad (\text{A2})$$

where  $\rho$  is the density at the substellar point of the planet, and

$$\sigma \equiv 2\pi I_1(\varepsilon_\rho) e^{-\varepsilon_\rho} H_\rho R_p \quad (\text{A3})$$

is the effective cross section of the planet, where  $I_1$  is the modified Bessel function of the first kind. If the flow is heterogeneous on scales smaller than the size of the planet ( $\varepsilon_\rho \gg 1$ ), then  $I_1(\varepsilon_\rho) \simeq \exp(\varepsilon_\rho) / \sqrt{2\pi\varepsilon_\rho}$ , and the effective cross section of the planet becomes (see also [B. D. Metzger et al. 2012](#))

$$\sigma \simeq \sqrt{2\pi} H_\rho^{3/2} R_p^{1/2} = \sqrt{2\pi} \varepsilon_\rho^{-3/2} R_p^2. \quad (\text{A4})$$

In contrast, when the density is approximately constant across the planet ( $\varepsilon_\rho \ll 1$ ), then  $I_1(\varepsilon_\rho) \approx \varepsilon_\rho/2$ , and the effective cross section approaches the typical value

$$\sigma \approx \pi R_p^2. \quad (\text{A5})$$

Figure 2 shows that during the surface interaction,  $\varepsilon_\rho > 1$ , such that equation (A4) is the effective cross section of the planet.

## B. COOLING ENVELOPE MODEL

[R. Tylenda \(2005\)](#) derived a differential equation for the evolution of a contracting polytropic envelope. See their Appendix A for a derivation. [R. Tylenda \(2005\)](#) showed that the differential equation for the radius of the envelope is (their equations (A.18 and A.19))

$$\frac{8\pi R_{\text{env}}^3 \sigma_{\text{SB}} T_{\text{eff}}^4}{GM_{\text{env}} M_\star} = \left[ \frac{d}{dt} \left( \frac{I_e}{I_m} \right) - \frac{\dot{R}_{\text{env}}}{R_{\text{env}}} \frac{I_e}{I_m} \right]. \quad (\text{B6})$$

Here,  $R_{\text{env}}$  is the radius of the envelope,  $\sigma_{\text{SB}}$  is the Stefan–Boltzmann constant,  $T_{\text{eff}}$  is the effective temperature of the envelope,  $M_{\text{env}}$  is the mass of the envelope, and

$$I_e \equiv \int_{x_\star}^1 (1-x)^n x^{1-n} dx, \quad (\text{B7})$$

$$I_m \equiv \int_{x_\star}^1 (1-x)^n x^{2-n} dx, \quad (\text{B8})$$

where  $x_\star \equiv R_\star/R_{\text{env}}$ . We can simplify equation (B6) by using

$$\frac{d}{dR_{\text{env}}} \int_{x_\star}^1 f(x) dx = \frac{x_\star}{R_{\text{env}}} f(x_\star), \quad (\text{B9})$$

from which we obtain

$$\frac{dI_e}{dR_{\text{env}}} = R_{\text{env}}^{-1} (1-x_\star)^n x_\star^{2-n}, \quad (\text{B10})$$

$$\frac{dI_m}{dR_{\text{env}}} = R_{\text{env}}^{-1} (1-x_\star)^n x_\star^{3-n}. \quad (\text{B11})$$

Using these relations, we can rewrite equation (B6) as

$$\dot{R}_{\text{env}} = -\frac{R_{\text{env}}}{t_{\text{KH,env}}} \frac{1}{g(x_\star)}, \quad (\text{B12})$$

where

$$g(x_\star) \equiv \frac{I_e}{I_m} + \frac{I_e}{I_m^2} (1-x_\star)^n x_\star^{3-n} - \frac{(1-x_\star)^n x_\star^{2-n}}{I_m} \quad (\text{B13})$$

and

$$t_{\text{KH,env}} \equiv \frac{GM_{\text{env}} M_\star}{8\pi R_{\text{env}}^3 \sigma_{\text{SB}} T_{\text{eff}}^4}. \quad (\text{B14})$$

## REFERENCES

- Adamów, M., Niedzielski, A., Villaver, E., Nowak, G., & Wolszczan, A. 2012, *ApJL*, 754, L15, doi: [10.1088/2041-8205/754/1/L15](#)
- Aguilera-Gómez, C., Chanamé, J., & Pinsonneault, M. H. 2020, *ApJL*, 897, L20, doi: [10.3847/2041-8213/ab9d26](#)
- Aguilera-Gómez, C., Chanamé, J., Pinsonneault, M. H., & Carlberg, J. K. 2016a, *ApJL*, 833, L24, doi: [10.3847/2041-8213/833/2/L24](#)
- Aguilera-Gómez, C., Chanamé, J., Pinsonneault, M. H., & Carlberg, J. K. 2016b, *ApJ*, 829, 127, doi: [10.3847/0004-637X/829/2/127](#)
- Alexander, J. B. 1967, *The Observatory*, 87, 238
- Angulo, C., Arnould, M., Rayet, M., et al. 1999, *NuPhA*, 656, 3, doi: [10.1016/S0375-9474\(99\)00030-5](#)
- Bailey, A., & Goodman, J. 2019, *MNRAS*, 482, 1872, doi: [10.1093/mnras/sty2805](#)

- Barker, A. J. 2020, MNRAS, 498, 2270, doi: [10.1093/mnras/staa2405](https://doi.org/10.1093/mnras/staa2405)
- Barker, A. J., Efroimsky, M., Makarov, V. V., & Veras, D. 2024, MNRAS, 527, 5131, doi: [10.1093/mnras/stad3530](https://doi.org/10.1093/mnras/stad3530)
- Bear, E., Kashi, A., & Soker, N. 2011, MNRAS, 416, 1965, doi: [10.1111/j.1365-2966.2011.19171.x](https://doi.org/10.1111/j.1365-2966.2011.19171.x)
- Bear, E., & Soker, N. 2011, MNRAS, 414, 1788, doi: [10.1111/j.1365-2966.2011.18527.x](https://doi.org/10.1111/j.1365-2966.2011.18527.x)
- Behmard, A., Dai, F., Brewer, J. M., Berger, T. A., & Howard, A. W. 2023, MNRAS, 521, 2969, doi: [10.1093/mnras/stad745](https://doi.org/10.1093/mnras/stad745)
- Blouin, S., Shaffer, N. R., Saumon, D., & Starrett, C. E. 2020, ApJ, 899, 46, doi: [10.3847/1538-4357/ab9e75](https://doi.org/10.3847/1538-4357/ab9e75)
- Boyajian, T. S., LaCourse, D. M., Rappaport, S. A., et al. 2016, MNRAS, 457, 3988, doi: [10.1093/mnras/stw218](https://doi.org/10.1093/mnras/stw218)
- Cabezón, R. M., Abia, C., Domínguez, I., & García-Senz, D. 2023, A&A, 670, A155, doi: [10.1051/0004-6361/202244848](https://doi.org/10.1051/0004-6361/202244848)
- Cameron, A. G. W., & Fowler, W. A. 1971, ApJ, 164, 111, doi: [10.1086/150821](https://doi.org/10.1086/150821)
- Carlberg, J. K., Cunha, K., Smith, V. V., & Majewski, S. R. 2012, ApJ, 757, 109, doi: [10.1088/0004-637X/757/2/109](https://doi.org/10.1088/0004-637X/757/2/109)
- Carlberg, J. K., Cunha, K., Smith, V. V., & Majewski, S. R. 2013, Astronomische Nachrichten, 334, 120, doi: [10.1002/asna.201211757](https://doi.org/10.1002/asna.201211757)
- Carlberg, J. K., Majewski, S. R., & Arras, P. 2009, ApJ, 700, 832, doi: [10.1088/0004-637X/700/1/832](https://doi.org/10.1088/0004-637X/700/1/832)
- Carlberg, J. K., Majewski, S. R., Arras, P., et al. 2011, in American Institute of Physics Conference Series, Vol. 1331, Planetary Systems Beyond the Main Sequence, ed. S. Schuh, H. Drechsel, & U. Heber (AIP), 33–40, doi: [10.1063/1.3556182](https://doi.org/10.1063/1.3556182)
- Carlberg, J. K., Smith, V. V., Cunha, K., Majewski, S. R., & Rood, R. T. 2010, ApJL, 723, L103, doi: [10.1088/2041-8205/723/1/L103](https://doi.org/10.1088/2041-8205/723/1/L103)
- Casey, A. R., Ho, A. Y. Q., Ness, M., et al. 2019, ApJ, 880, 125, doi: [10.3847/1538-4357/ab27bf](https://doi.org/10.3847/1538-4357/ab27bf)
- Cassisi, S., Potekhin, A. Y., Pietrinferni, A., Catelan, M., & Salaris, M. 2007, ApJ, 661, 1094, doi: [10.1086/516819](https://doi.org/10.1086/516819)
- Chambers, K. C., Magnier, E. A., Metcalfe, N., et al. 2016, arXiv e-prints, arXiv:1612.05560, doi: [10.48550/arXiv.1612.05560](https://doi.org/10.48550/arXiv.1612.05560)
- Chugunov, A. I., Dewitt, H. E., & Yakovlev, D. G. 2007, PhRvD, 76, 025028, doi: [10.1103/PhysRevD.76.025028](https://doi.org/10.1103/PhysRevD.76.025028)
- Church, R. P., Mustill, A. J., & Liu, F. 2020, MNRAS, 491, 2391, doi: [10.1093/mnras/stz3169](https://doi.org/10.1093/mnras/stz3169)
- Cody, A. M., & Sasselov, D. D. 2005, ApJ, 622, 704, doi: [10.1086/427909](https://doi.org/10.1086/427909)
- Cyburt, R. H., Amthor, A. M., Ferguson, R., et al. 2010, ApJS, 189, 240, doi: [10.1088/0067-0049/189/1/240](https://doi.org/10.1088/0067-0049/189/1/240)
- Damiani, C., & Díaz, R. F. 2016, A&A, 589, A55, doi: [10.1051/0004-6361/201527100](https://doi.org/10.1051/0004-6361/201527100)
- De, K., MacLeod, M., Karambelkar, V., et al. 2023, Nature, 617, 55, doi: [10.1038/s41586-023-05842-x](https://doi.org/10.1038/s41586-023-05842-x)
- Faber, J. A., Rasio, F. A., & Willems, B. 2005, Icarus, 175, 248, doi: [10.1016/j.icarus.2004.10.021](https://doi.org/10.1016/j.icarus.2004.10.021)
- Ferguson, J. W., Alexander, D. R., Allard, F., et al. 2005, ApJ, 623, 585, doi: [10.1086/428642](https://doi.org/10.1086/428642)
- Fuller, G. M., Fowler, W. A., & Newman, M. J. 1985, ApJ, 293, 1, doi: [10.1086/163208](https://doi.org/10.1086/163208)
- Gaia Collaboration, Prusti, T., de Bruijne, J. H. J., et al. 2016, A&A, 595, A1, doi: [10.1051/0004-6361/201629272](https://doi.org/10.1051/0004-6361/201629272)
- Gaia Collaboration, Brown, A. G. A., Vallenari, A., et al. 2021, A&A, 649, A1, doi: [10.1051/0004-6361/202039657](https://doi.org/10.1051/0004-6361/202039657)
- Goldbaum, N. J., ZuHone, J. A., Turk, M. J., Kowalik, K., & Rosen, A. L. 2018, Journal of Open Source Software, 3, 809, doi: [10.21105/joss.00809](https://doi.org/10.21105/joss.00809)
- Gratton, R. G., Bonanno, G., Claudi, R. U., et al. 2001, A&A, 377, 123, doi: [10.1051/0004-6361:20011066](https://doi.org/10.1051/0004-6361:20011066)
- Guillochon, J., Ramirez-Ruiz, E., & Lin, D. 2011, ApJ, 732, 74, doi: [10.1088/0004-637X/732/2/74](https://doi.org/10.1088/0004-637X/732/2/74)
- Guo, S.-S. 2023, Research in Astronomy and Astrophysics, 23, 095014, doi: [10.1088/1674-4527/ace028](https://doi.org/10.1088/1674-4527/ace028)
- Hamer, J. H., & Schlaufman, K. C. 2019, AJ, 158, 190, doi: [10.3847/1538-3881/ab3c56](https://doi.org/10.3847/1538-3881/ab3c56)
- Harris, C. R., Millman, K. J., van der Walt, S. J., et al. 2020, Nature, 585, 357–362, doi: [10.1038/s41586-020-2649-2](https://doi.org/10.1038/s41586-020-2649-2)
- Hartman, J. D., Bakos, G. Á., Bhatti, W., et al. 2016, AJ, 152, 182, doi: [10.3847/0004-6256/152/6/182](https://doi.org/10.3847/0004-6256/152/6/182)
- Hartmann, L., Herczeg, G., & Calvet, N. 2016, ARA&A, 54, 135, doi: [10.1146/annurev-astro-081915-023347](https://doi.org/10.1146/annurev-astro-081915-023347)
- Herczeg, G. J., Dong, S., Shappee, B. J., et al. 2016, ApJ, 831, 133, doi: [10.3847/0004-637X/831/2/133](https://doi.org/10.3847/0004-637X/831/2/133)
- Howard, A. W., Marcy, G. W., Bryson, S. T., et al. 2012, ApJS, 201, 15, doi: [10.1088/0067-0049/201/2/15](https://doi.org/10.1088/0067-0049/201/2/15)
- Hunter, J. D. 2007, Computing in Science & Engineering, 9, 90, doi: [10.1109/MCSE.2007.55](https://doi.org/10.1109/MCSE.2007.55)
- Hutchinson-Smith, T., Everson, R. W., Twum, A. A., et al. 2024, ApJ, 977, 196, doi: [10.3847/1538-4357/ad88f3](https://doi.org/10.3847/1538-4357/ad88f3)
- Iglesias, C. A., & Rogers, F. J. 1993, ApJ, 412, 752, doi: [10.1086/172958](https://doi.org/10.1086/172958)
- Iglesias, C. A., & Rogers, F. J. 1996, ApJ, 464, 943, doi: [10.1086/177381](https://doi.org/10.1086/177381)
- Irwin, A. W. 2004, <http://freeeos.sourceforge.net/>
- Israelian, G., Santos, N. C., Mayor, M., & Rebolo, R. 2001, Nature, 411, 163, doi: [10.1038/35075512](https://doi.org/10.1038/35075512)
- Itoh, N., Hayashi, H., Nishikawa, A., & Kohyama, Y. 1996, ApJS, 102, 411, doi: [10.1086/192264](https://doi.org/10.1086/192264)

- Ivanova, N., Justham, S., Avendano Nandez, J. L., & Lombardi, J. C. 2013, *Science*, 339, 433, doi: [10.1126/science.1225540](https://doi.org/10.1126/science.1225540)
- Jackson, B., Barnes, R., & Greenberg, R. 2009, *ApJ*, 698, 1357, doi: [10.1088/0004-637X/698/2/1357](https://doi.org/10.1088/0004-637X/698/2/1357)
- Jackson, B., Jensen, E., Peacock, S., Arras, P., & Penev, K. 2016, *Celestial Mechanics and Dynamical Astronomy*, 126, 227, doi: [10.1007/s10569-016-9704-1](https://doi.org/10.1007/s10569-016-9704-1)
- Jermyn, A. S., Schwab, J., Bauer, E., Timmes, F. X., & Potekhin, A. Y. 2021, *ApJ*, 913, 72, doi: [10.3847/1538-4357/abf48e](https://doi.org/10.3847/1538-4357/abf48e)
- Jermyn, A. S., Bauer, E. B., Schwab, J., et al. 2023, *ApJS*, 265, 15, doi: [10.3847/1538-4365/acae8d](https://doi.org/10.3847/1538-4365/acae8d)
- Jia, S., & Spruit, H. C. 2018, *ApJ*, 864, 169, doi: [10.3847/1538-4357/aad77c](https://doi.org/10.3847/1538-4357/aad77c)
- Kane, S. R. 2023, *ApJ*, 958, 120, doi: [10.3847/1538-4357/ad06b2](https://doi.org/10.3847/1538-4357/ad06b2)
- Kashi, A. 2018, *Galaxies*, 6, 82, doi: [10.3390/galaxies6030082](https://doi.org/10.3390/galaxies6030082)
- Kashi, A., Michaelis, A. M., & Feigin, L. 2019, *Galaxies*, 8, 2, doi: [10.3390/galaxies8010002](https://doi.org/10.3390/galaxies8010002)
- Kashi, A., & Soker, N. 2017, *MNRAS*, 468, 4938, doi: [10.1093/mnras/stx767](https://doi.org/10.1093/mnras/stx767)
- Komacek, T. D., & Youdin, A. N. 2017, *ApJ*, 844, 94, doi: [10.3847/1538-4357/aa7b75](https://doi.org/10.3847/1538-4357/aa7b75)
- Kramer, M., Schneider, F. R. N., Ohlmann, S. T., et al. 2020, *A&A*, 642, A97, doi: [10.1051/0004-6361/202038702](https://doi.org/10.1051/0004-6361/202038702)
- Kunitomo, M., Ikoma, M., Sato, B., Katsuta, Y., & Ida, S. 2011, *ApJ*, 737, 66, doi: [10.1088/0004-637X/737/2/66](https://doi.org/10.1088/0004-637X/737/2/66)
- Langanke, K., & Martínez-Pinedo, G. 2000, *NuPhA*, 673, 481, doi: [10.1016/S0375-9474\(00\)00131-7](https://doi.org/10.1016/S0375-9474(00)00131-7)
- Lau, M. Y. M., Cantiello, M., Jermyn, A. S., et al. 2025, *A&A*, 694, A264, doi: [10.1051/0004-6361/202452081](https://doi.org/10.1051/0004-6361/202452081)
- Lau, R. M., Jencson, J. E., Salyk, C., et al. 2025, *ApJ*, 983, 87, doi: [10.3847/1538-4357/adb429](https://doi.org/10.3847/1538-4357/adb429)
- Laughlin, G., & Adams, F. C. 1997, *ApJL*, 491, L51, doi: [10.1086/311056](https://doi.org/10.1086/311056)
- Lawrence, A., Warren, S. J., Almaini, O., et al. 2007, *MNRAS*, 379, 1599, doi: [10.1111/j.1365-2966.2007.12040.x](https://doi.org/10.1111/j.1365-2966.2007.12040.x)
- Lazovik, Y. A. 2023, *MNRAS*, 520, 3749, doi: [10.1093/mnras/stad394](https://doi.org/10.1093/mnras/stad394)
- Leonardi, P., Nascimbeni, V., Granata, V., et al. 2024, *A&A*, 686, A84, doi: [10.1051/0004-6361/202348363](https://doi.org/10.1051/0004-6361/202348363)
- Levrard, B., Winisdoerffer, C., & Chabrier, G. 2009, *ApJL*, 692, L9, doi: [10.1088/0004-637X/692/1/L9](https://doi.org/10.1088/0004-637X/692/1/L9)
- Li, S. L., Lin, D. N. C., & Liu, X. W. 2008, *ApJ*, 685, 1210, doi: [10.1086/591122](https://doi.org/10.1086/591122)
- Liu, F., Ting, Y.-S., Yong, D., et al. 2024, *Nature*, 627, 501, doi: [10.1038/s41586-024-07091-y](https://doi.org/10.1038/s41586-024-07091-y)
- Liu, S.-F., Guillochon, J., Lin, D. N. C., & Ramirez-Ruiz, E. 2013, *ApJ*, 762, 37, doi: [10.1088/0004-637X/762/1/37](https://doi.org/10.1088/0004-637X/762/1/37)
- Livio, M., & Soker, N. 2002, *ApJL*, 571, L161, doi: [10.1086/341411](https://doi.org/10.1086/341411)
- Lopez, E. D., & Fortney, J. J. 2016, *ApJ*, 818, 4, doi: [10.3847/0004-637X/818/1/4](https://doi.org/10.3847/0004-637X/818/1/4)
- Maciejewski, G., Dimitrov, D., Fernández, M., et al. 2016, *A&A*, 588, L6, doi: [10.1051/0004-6361/201628312](https://doi.org/10.1051/0004-6361/201628312)
- Maciejewski, G., Fernández, M., Aceituno, F., et al. 2018, *AcA*, 68, 371, doi: [10.32023/0001-5237/68.4.4](https://doi.org/10.32023/0001-5237/68.4.4)
- MacLeod, M., Cantiello, M., & Soares-Furtado, M. 2018a, *ApJL*, 853, L1, doi: [10.3847/2041-8213/aaa5fa](https://doi.org/10.3847/2041-8213/aaa5fa)
- MacLeod, M., & Loeb, A. 2020, *ApJ*, 895, 29, doi: [10.3847/1538-4357/ab89b6](https://doi.org/10.3847/1538-4357/ab89b6)
- MacLeod, M., Macias, P., Ramirez-Ruiz, E., et al. 2017, *ApJ*, 835, 282, doi: [10.3847/1538-4357/835/2/282](https://doi.org/10.3847/1538-4357/835/2/282)
- MacLeod, M., Ostriker, E. C., & Stone, J. M. 2018b, *ApJ*, 863, 5, doi: [10.3847/1538-4357/aacf08](https://doi.org/10.3847/1538-4357/aacf08)
- Massarotti, A., Latham, D. W., Stefanik, R. P., & Fogel, J. 2008, *AJ*, 135, 209, doi: [10.1088/0004-6256/135/1/209](https://doi.org/10.1088/0004-6256/135/1/209)
- Matsakos, T., & Königl, A. 2015, *ApJL*, 809, L20, doi: [10.1088/2041-8205/809/2/L20](https://doi.org/10.1088/2041-8205/809/2/L20)
- Matsumoto, T., & Metzger, B. D. 2022, *ApJ*, 938, 5, doi: [10.3847/1538-4357/ac6269](https://doi.org/10.3847/1538-4357/ac6269)
- Matsumura, S., Peale, S. J., & Rasio, F. A. 2010, *ApJ*, 725, 1995, doi: [10.1088/0004-637X/725/2/1995](https://doi.org/10.1088/0004-637X/725/2/1995)
- McKinney, W. 2010, in *Proceedings of the 9th Python in Science Conference*, ed. Stéfan van der Walt & Jarrod Millman, 56 – 61, doi: [10.25080/Majora-92bf1922-00a](https://doi.org/10.25080/Majora-92bf1922-00a)
- Metzger, B. D., Giannios, D., & Spiegel, D. S. 2012, *MNRAS*, 425, 2778, doi: [10.1111/j.1365-2966.2012.21444.x](https://doi.org/10.1111/j.1365-2966.2012.21444.x)
- Metzger, B. D., Shen, K. J., & Stone, N. 2017, *MNRAS*, 468, 4399, doi: [10.1093/mnras/stx823](https://doi.org/10.1093/mnras/stx823)
- Millholland, S. C., MacLeod, M., & Xiao, F. 2025, *ApJ*, 981, 77, doi: [10.3847/1538-4357/ada76d](https://doi.org/10.3847/1538-4357/ada76d)
- Miquelarena, P., Saffe, C., Flores, M., et al. 2024, *A&A*, 688, A73, doi: [10.1051/0004-6361/202449983](https://doi.org/10.1051/0004-6361/202449983)
- Miyazaki, S., & Masuda, K. 2023, *AJ*, 166, 209, doi: [10.3847/1538-3881/acff71](https://doi.org/10.3847/1538-3881/acff71)
- Montalbán, J., & Rebolo, R. 2002, *A&A*, 386, 1039, doi: [10.1051/0004-6361:20020338](https://doi.org/10.1051/0004-6361:20020338)
- Murray, S. D., White, S. D. M., Blondin, J. M., & Lin, D. N. C. 1993, *ApJ*, 407, 588, doi: [10.1086/172540](https://doi.org/10.1086/172540)
- Murray-Clay, R. A., Chiang, E. I., & Murray, N. 2009, *ApJ*, 693, 23, doi: [10.1088/0004-637X/693/1/23](https://doi.org/10.1088/0004-637X/693/1/23)
- Mustill, A. 2024, *arXiv e-prints*, arXiv:2405.09399, doi: [10.48550/arXiv.2405.09399](https://doi.org/10.48550/arXiv.2405.09399)
- Mustill, A. J., & Villaver, E. 2012, *ApJ*, 761, 121, doi: [10.1088/0004-637X/761/2/121](https://doi.org/10.1088/0004-637X/761/2/121)
- Nagar, T., Spina, L., & Karakas, A. I. 2020, *ApJL*, 888, L9, doi: [10.3847/2041-8213/ab5dc6](https://doi.org/10.3847/2041-8213/ab5dc6)

- Nordhaus, J., & Spiegel, D. S. 2013, *MNRAS*, 432, 500, doi: [10.1093/mnras/stt569](https://doi.org/10.1093/mnras/stt569)
- Nordhaus, J., Spiegel, D. S., Ibgui, L., Goodman, J., & Burrows, A. 2010, *MNRAS*, 408, 631, doi: [10.1111/j.1365-2966.2010.17155.x](https://doi.org/10.1111/j.1365-2966.2010.17155.x)
- O'Connor, C. E., Bildsten, L., Cantiello, M., & Lai, D. 2023, *ApJ*, 950, 128, doi: [10.3847/1538-4357/acd2d4](https://doi.org/10.3847/1538-4357/acd2d4)
- O'Connor, C. E., & Lai, D. 2025, *ApJL*, 978, L26, doi: [10.3847/2041-8213/ada1ce](https://doi.org/10.3847/2041-8213/ada1ce)
- Oda, T., Hino, M., Muto, K., Takahara, M., & Sato, K. 1994, *Atomic Data and Nuclear Data Tables*, 56, 231, doi: [10.1006/adnd.1994.1007](https://doi.org/10.1006/adnd.1994.1007)
- Oetjens, A., Carone, L., Bergemann, M., & Serenelli, A. 2020, *A&A*, 643, A34, doi: [10.1051/0004-6361/202038653](https://doi.org/10.1051/0004-6361/202038653)
- Ogilvie, G. I. 2014, *ARA&A*, 52, 171, doi: [10.1146/annurev-astro-081913-035941](https://doi.org/10.1146/annurev-astro-081913-035941)
- Oh, S., Price-Whelan, A. M., Brewer, J. M., et al. 2018, *ApJ*, 854, 138, doi: [10.3847/1538-4357/aaab4d](https://doi.org/10.3847/1538-4357/aaab4d)
- Passy, J.-C., Mac Low, M.-M., & De Marco, O. 2012, *ApJL*, 759, L30, doi: [10.1088/2041-8205/759/2/L30](https://doi.org/10.1088/2041-8205/759/2/L30)
- Patra, K. C., Winn, J. N., Holman, M. J., et al. 2017, *AJ*, 154, 4, doi: [10.3847/1538-3881/aa6d75](https://doi.org/10.3847/1538-3881/aa6d75)
- Paxton, B., Bildsten, L., Dotter, A., et al. 2011, *ApJS*, 192, 3, doi: [10.1088/0067-0049/192/1/3](https://doi.org/10.1088/0067-0049/192/1/3)
- Paxton, B., Cantiello, M., Arras, P., et al. 2013, *ApJS*, 208, 4, doi: [10.1088/0067-0049/208/1/4](https://doi.org/10.1088/0067-0049/208/1/4)
- Paxton, B., Marchant, P., Schwab, J., et al. 2015, *ApJS*, 220, 15, doi: [10.1088/0067-0049/220/1/15](https://doi.org/10.1088/0067-0049/220/1/15)
- Paxton, B., Schwab, J., Bauer, E. B., et al. 2018, *ApJS*, 234, 34, doi: [10.3847/1538-4365/aaa5a8](https://doi.org/10.3847/1538-4365/aaa5a8)
- Paxton, B., Smolec, R., Schwab, J., et al. 2019, *ApJS*, 243, 10, doi: [10.3847/1538-4365/ab2241](https://doi.org/10.3847/1538-4365/ab2241)
- Penev, K., Bouma, L. G., Winn, J. N., & Hartman, J. D. 2018, *AJ*, 155, 165, doi: [10.3847/1538-3881/aaaf71](https://doi.org/10.3847/1538-3881/aaaf71)
- Podsiadlowski, P. 1996, *MNRAS*, 279, 1104, doi: [10.1093/mnras/279.4.1104](https://doi.org/10.1093/mnras/279.4.1104)
- Popkov, A. V., & Popov, S. B. 2019, *MNRAS*, 490, 2390, doi: [10.1093/mnras/stz2783](https://doi.org/10.1093/mnras/stz2783)
- Potekhin, A. Y., & Chabrier, G. 2010, *Contributions to Plasma Physics*, 50, 82, doi: [10.1002/ctpp.201010017](https://doi.org/10.1002/ctpp.201010017)
- Poutanen, J. 2017, *ApJ*, 835, 119, doi: [10.3847/1538-4357/835/2/119](https://doi.org/10.3847/1538-4357/835/2/119)
- Privitera, G., Meynet, G., Eggenberger, P., et al. 2016a, *A&A*, 593, A128, doi: [10.1051/0004-6361/201628758](https://doi.org/10.1051/0004-6361/201628758)
- Privitera, G., Meynet, G., Eggenberger, P., et al. 2016b, *A&A*, 591, A45, doi: [10.1051/0004-6361/201528044](https://doi.org/10.1051/0004-6361/201528044)
- Privitera, G., Meynet, G., Eggenberger, P., et al. 2016c, *A&A*, 593, L15, doi: [10.1051/0004-6361/201629142](https://doi.org/10.1051/0004-6361/201629142)
- Qureshi, A., Naoz, S., & Shkolnik, E. L. 2018, *ApJ*, 864, 65, doi: [10.3847/1538-4357/aad562](https://doi.org/10.3847/1538-4357/aad562)
- Rapoport, I., Bear, E., & Soker, N. 2021, *MNRAS*, 506, 468, doi: [10.1093/mnras/stab1774](https://doi.org/10.1093/mnras/stab1774)
- Rasio, F. A., Tout, C. A., Lubow, S. H., & Livio, M. 1996, *ApJ*, 470, 1187, doi: [10.1086/177941](https://doi.org/10.1086/177941)
- Reid, I. N., Brewer, C., Brucato, R. J., et al. 1991, *PASP*, 103, 661, doi: [10.1086/132866](https://doi.org/10.1086/132866)
- Rogers, F. J., & Nayfonov, A. 2002, *ApJ*, 576, 1064, doi: [10.1086/341894](https://doi.org/10.1086/341894)
- Saffe, C., Jofré, E., Martioli, E., et al. 2017, *A&A*, 604, L4, doi: [10.1051/0004-6361/201731430](https://doi.org/10.1051/0004-6361/201731430)
- Saffe, C., Miquelarena, P., Alacoria, J., et al. 2024, *A&A*, 682, L23, doi: [10.1051/0004-6361/202449263](https://doi.org/10.1051/0004-6361/202449263)
- Sandquist, E., Taam, R. E., Lin, D. N. C., & Burkert, A. 1998, *ApJL*, 506, L65, doi: [10.1086/311633](https://doi.org/10.1086/311633)
- Sandquist, E. L., Dokter, J. J., Lin, D. N. C., & Mardling, R. A. 2002, *ApJ*, 572, 1012, doi: [10.1086/340452](https://doi.org/10.1086/340452)
- Saumon, D., Chabrier, G., & van Horn, H. M. 1995, *ApJS*, 99, 713, doi: [10.1086/192204](https://doi.org/10.1086/192204)
- Sayeed, M., Ness, M. K., Montet, B. T., et al. 2024, *ApJ*, 964, 42, doi: [10.3847/1538-4357/ad1936](https://doi.org/10.3847/1538-4357/ad1936)
- Schlaufman, K. C., & Winn, J. N. 2013, *ApJ*, 772, 143, doi: [10.1088/0004-637X/772/2/143](https://doi.org/10.1088/0004-637X/772/2/143)
- Schwab, J., Wolf, B., Zingale, M., et al. 2024, 0.3.5 Zenodo, doi: [10.5281/zenodo.13697200](https://doi.org/10.5281/zenodo.13697200)
- Sevilla, J., Behmard, A., & Fuller, J. 2022, *MNRAS*, 516, 3354, doi: [10.1093/mnras/stac2436](https://doi.org/10.1093/mnras/stac2436)
- Sicilia-Aguilar, A., Oprandi, A., Froebrich, D., et al. 2017, *A&A*, 607, A127, doi: [10.1051/0004-6361/201731263](https://doi.org/10.1051/0004-6361/201731263)
- Siess, L., & Livio, M. 1999a, *MNRAS*, 304, 925, doi: [10.1046/j.1365-8711.1999.02376.x](https://doi.org/10.1046/j.1365-8711.1999.02376.x)
- Siess, L., & Livio, M. 1999b, *MNRAS*, 308, 1133, doi: [10.1046/j.1365-8711.1999.02784.x](https://doi.org/10.1046/j.1365-8711.1999.02784.x)
- Soares, B. M. T. B., Adibekyan, V., Mordasini, C., et al. 2025, *A&A*, 693, A47, doi: [10.1051/0004-6361/202451399](https://doi.org/10.1051/0004-6361/202451399)
- Soares-Furtado, M., Cantiello, M., MacLeod, M., & Ness, M. K. 2021, *AJ*, 162, 273, doi: [10.3847/1538-3881/ac273c](https://doi.org/10.3847/1538-3881/ac273c)
- Soker, N. 2020, *ApJ*, 893, 20, doi: [10.3847/1538-4357/ab7dbb](https://doi.org/10.3847/1538-4357/ab7dbb)
- Soker, N. 2023, *MNRAS*, 524, L94, doi: [10.1093/mnras/slado86](https://doi.org/10.1093/mnras/slado86)
- Soker, N., & Kaplan, N. 2021, *Research in Astronomy and Astrophysics*, 21, 090, doi: [10.1088/1674-4527/21/4/90](https://doi.org/10.1088/1674-4527/21/4/90)
- Soker, N., & Tylenda, R. 2006, *MNRAS*, 373, 733, doi: [10.1111/j.1365-2966.2006.11056.x](https://doi.org/10.1111/j.1365-2966.2006.11056.x)
- Soliman, N. H., & Hopkins, P. F. 2025, *ApJ*, 979, 98, doi: [10.3847/1538-4357/ada1d5](https://doi.org/10.3847/1538-4357/ada1d5)
- Spina, L., Palla, F., Randich, S., et al. 2015, *A&A*, 582, L6, doi: [10.1051/0004-6361/201526896](https://doi.org/10.1051/0004-6361/201526896)
- Staff, J. E., De Marco, O., Wood, P., Galaviz, P., & Passy, J.-C. 2016, *MNRAS*, 458, 832, doi: [10.1093/mnras/stw331](https://doi.org/10.1093/mnras/stw331)

- Stephan, A. P., Naoz, S., Gaudi, B. S., & Salas, J. M. 2020, *ApJ*, 889, 45, doi: [10.3847/1538-4357/ab5b00](https://doi.org/10.3847/1538-4357/ab5b00)
- Sun, Q., Ting, Y.-S., Liu, F., et al. 2025, *ApJ*, 978, 107, doi: [10.3847/1538-4357/ad8dc3](https://doi.org/10.3847/1538-4357/ad8dc3)
- Tejada Arevalo, R. A., Winn, J. N., & Anderson, K. R. 2021, *ApJ*, 919, 138, doi: [10.3847/1538-4357/ac1429](https://doi.org/10.3847/1538-4357/ac1429)
- Thorngren, D. P., Fortney, J. J., Lopez, E. D., Berger, T. A., & Huber, D. 2021, *ApJL*, 909, L16, doi: [10.3847/2041-8213/abe86d](https://doi.org/10.3847/2041-8213/abe86d)
- Thorngren, D. P., Lee, E. J., & Lopez, E. D. 2023, *ApJL*, 945, L36, doi: [10.3847/2041-8213/acbd35](https://doi.org/10.3847/2041-8213/acbd35)
- Timmes, F. X., & Swesty, F. D. 2000, *ApJS*, 126, 501, doi: [10.1086/313304](https://doi.org/10.1086/313304)
- Tognelli, E., Prada Moroni, P. G., & Degl’Innocenti, S. 2016, *MNRAS*, 460, 3888, doi: [10.1093/mnras/stw1268](https://doi.org/10.1093/mnras/stw1268)
- Townsend, R. 2024,, 24.7.1 Zenodo, doi: [10.5281/zenodo.13768941](https://doi.org/10.5281/zenodo.13768941)
- Turner, J. D., Ridden-Harper, A., & Jayawardhana, R. 2021, *AJ*, 161, 72, doi: [10.3847/1538-3881/abd178](https://doi.org/10.3847/1538-3881/abd178)
- Tylenda, R. 2005, *A&A*, 436, 1009, doi: [10.1051/0004-6361:20052800](https://doi.org/10.1051/0004-6361:20052800)
- Tylenda, R., Crause, L. A., Górny, S. K., & Schmidt, M. R. 2005, *A&A*, 439, 651, doi: [10.1051/0004-6361:20041581](https://doi.org/10.1051/0004-6361:20041581)
- Tylenda, R., Hajduk, M., Kamiński, T., et al. 2011, *A&A*, 528, A114, doi: [10.1051/0004-6361/201016221](https://doi.org/10.1051/0004-6361/201016221)
- Valsecchi, F., Rappaport, S., Rasio, F. A., Marchant, P., & Rogers, L. A. 2015, *ApJ*, 813, 101, doi: [10.1088/0004-637X/813/2/101](https://doi.org/10.1088/0004-637X/813/2/101)
- Valsecchi, F., Rasio, F. A., & Steffen, J. H. 2014, *ApJL*, 793, L3, doi: [10.1088/2041-8205/793/1/L3](https://doi.org/10.1088/2041-8205/793/1/L3)
- Veras, D. 2016, *Royal Society Open Science*, 3, 150571, doi: [10.1098/rsos.150571](https://doi.org/10.1098/rsos.150571)
- Villaver, E., & Livio, M. 2007, *ApJ*, 661, 1192, doi: [10.1086/516746](https://doi.org/10.1086/516746)
- Villaver, E., & Livio, M. 2009, *ApJL*, 705, L81, doi: [10.1088/0004-637X/705/1/L81](https://doi.org/10.1088/0004-637X/705/1/L81)
- Villaver, E., Livio, M., Mustill, A. J., & Siess, L. 2014, *ApJ*, 794, 3, doi: [10.1088/0004-637X/794/1/3](https://doi.org/10.1088/0004-637X/794/1/3)
- Virtanen, P., Gommers, R., Oliphant, T. E., et al. 2020, *Nature Methods*, 17, 261, doi: [10.1038/s41592-019-0686-2](https://doi.org/10.1038/s41592-019-0686-2)
- Vissapragada, S., Chontos, A., Greklek-McKeon, M., et al. 2022, *ApJL*, 941, L31, doi: [10.3847/2041-8213/aca47e](https://doi.org/10.3847/2041-8213/aca47e)
- Weinberg, N. N., Davachi, N., Essick, R., et al. 2024, *ApJ*, 960, 50, doi: [10.3847/1538-4357/ad05c9](https://doi.org/10.3847/1538-4357/ad05c9)
- Xie, D., Zhu, C., Guo, S., Liu, H., & Lü, G. 2023, *MNRAS*, 524, 3705, doi: [10.1093/mnras/stad2097](https://doi.org/10.1093/mnras/stad2097)
- Yamazaki, R., Hayasaki, K., & Loeb, A. 2017, *MNRAS*, 466, 1421, doi: [10.1093/mnras/stw3207](https://doi.org/10.1093/mnras/stw3207)
- Yan, H.-L., Shi, J.-R., Zhou, Y.-T., et al. 2018, *Nature Astronomy*, 2, 790, doi: [10.1038/s41550-018-0544-7](https://doi.org/10.1038/s41550-018-0544-7)
- Yana Galarza, J., López-Valdivia, R., Meléndez, J., & Lorenzo-Oliveira, D. 2021, *ApJ*, 922, 129, doi: [10.3847/1538-4357/ac2362](https://doi.org/10.3847/1538-4357/ac2362)
- Yana Galarza, J., Reggiani, H., Ferreira, T., et al. 2024, *ApJ*, 974, 122, doi: [10.3847/1538-4357/ad697f](https://doi.org/10.3847/1538-4357/ad697f)
- Yarza, R., Razo-López, N. B., Murguía-Berthier, A., et al. 2023, *ApJ*, 954, 176, doi: [10.3847/1538-4357/acbdfc](https://doi.org/10.3847/1538-4357/acbdfc)
- Yee, S. W., Winn, J. N., Knutson, H. A., et al. 2020, *ApJL*, 888, L5, doi: [10.3847/2041-8213/ab5c16](https://doi.org/10.3847/2041-8213/ab5c16)
- Zhang, M., & Penev, K. 2014, *ApJ*, 787, 131, doi: [10.1088/0004-637X/787/2/131](https://doi.org/10.1088/0004-637X/787/2/131)
- Zhu, W., & Dong, S. 2021, *ARA&A*, 59, 291, doi: [10.1146/annurev-astro-112420-020055](https://doi.org/10.1146/annurev-astro-112420-020055)